Available online at www.sciencedirect.com
ScienceDirect
Journal of Power Sources 170 (2007) 495–512
JOURNAL OF POWER SOURCES
www.elsevier.com/locate/jpowsour

Studies of the pulse charge of lead-acid batteries for PV applications Part II. Impedance of the positive plate revisited

A. Kirchev *, A. Delaille, M. Perrin, E. Lemaire, F. Mattera

Laboratoire des Systèmes Solaires, INES-RDI, BP 332, 73377 Le Bourget du Lac, 50, avenue du Lac Léman, France

Received 6 March 2007; accepted 20 March 2007
Available online 27 March 2007

Abstract

In the second part of this publication series, dedicated to the pulse charge of the lead-acid battery, a special attention is paid to the impedance spectrum of the positive plate as a source for estimation of the electrostatic capacitance of the double layer (C_{dl}) on the surface of the positive active mass. The impedance spectra were measured at open circuit for different states of charge (SoC) in H_2SO_4 with specific gravity 1.24 and 1.28 g ml^{-1}. A substantial difference was observed in the impedance spectra of partially charged and partially discharged positive plates keeping the same value of the SOC. The impedance data were subjected to inductance error correction, followed by differential impedance analysis (DIA). Considering the results from DIA, the recently published equivalent circuits of the positive plate in charged and in discharged state and the gel-crystal model of the lead dioxide, we proposed a model of the positive plate in partial state of charge (PSoC). The analysis of the obtained experimental results using this model and DIA show that the double layer capacitance is not frequency distributed. The influence of the state of charge and state of health on the model parameters is discussed. One of the most interesting results is the dependence of C_{dl} on SOC—it features a hysteresis at which the values of C_{dl} during the charge are 5–6 times higher than the corresponding ones during the discharge. This result was discussed in terms of changes in the double layer structure considering the gel-crystal model of the lead dioxide. During the discharge in H_2SO_4 with specific gravity 1.28 g ml^{-1} a passivation process was detected as a high frequency pseudo-inductive loop in the Nyquist plots in PSoC. The passivation time constant is higher at 50–60% SOC and decreases to zero in the end of the discharge. During the charge in both electrolytes, pseudo-inductive time constant was observed too. It was attributed to the phenomena of the dehydration of $Pb(OH)_4$, an intermediate in the reaction scheme of the $PbSO_4$ oxidation. The state of health influences mostly the ohmic resistance R_Ω, the charge transfer resistance R_{ct} and the parameters of the constant phase element accounting the diffusion in the pores (CPE_{diff}), when the plate is well charged.

Keywords: Lead-acid batteries; Positive plate; Gel-crystal model; Impedance spectroscopy (EIS); Electrochemical double layer (EDL); State of health (SoC); State of charge (SoH)

1. Introduction

In the first part of this work it was found that the electrochemical double layer (EDL) on the surface of the lead dioxide, constituting the positive active material (PAM) of the lead-acid battery, plays a very important role in the mechanism of the pulse charge [1]. Using the concept of the average double layer current, it was demonstrated that during the "ON" periods of the pulse charge, in some cases more than a half of the energy introduced in the charge of the positive plate can be used to charge the double layer instead of faradic processes like lead sulphate oxidation or oxygen evolution. The electrochemical impedance spectroscopy (EIS) is one of the best methods to study the EDL properties, especially in the case of high porosity systems like PAM, where methods like the linear sweep cyclic voltammetry are hardly applicable because of the high currents and the simultaneous proceeding of faradic processes. In addition, the impedance spectroscopy provides an opportunity for an *in situ* microstructural characterisation of the positive plate, and more

* Corresponding author at: INES-RDI, BP 332, 73377 Le Bourget du Lac, 50, avenue du Lac Léman, France. Tel.: +33 4 79 44 45 48; fax: +33 4 79 68 80 49.
E-mail address: angel.kirchev@cea.fr (A. Kirchev).

0378-7753/$ – see front matter © 2007 Elsevier B.V. All rights reserved.
doi:10.1016/j.jpowsour.2007.03.045

particularly the PbO_2/electrolyte interphase. EIS is also widely used as a tool for estimation of the state of charge (SoC) and state of health (SoH) of the battery [2–10].

The first studies of the EDL on the surface of the lead dioxide have been published more than half a century ago by Kiseleva and Kabanov [11]. The measured potential of the zero charge (PZC) in 0.05 M H_2SO_4 is about 1.8 V versus normal hydrogen electrode (NHE), which is more than 300 mV above the equilibrium value of the PbO_2/$PbSO_4$ electrode in 5 M H_2SO_4 (1.464 V versus NHE). The same authors estimate also a strong adsorption of sulphuric acid species (H_2SO_4, HSO_4^- and SO_4^{2-}) [12]. Later, Carr and Hampson extend the studies on the EDL of lead dioxide electrode towards less concentrated H_2SO_4 and estimate the presence of surface reactions with the participation of H^+ ions [13]. Recently Munichandraiah, using cyclic voltammetry, showed that the EDL capacitance increases substantially with the rise of the PbO_2 electrodeposition current density—from 10 mF cm^{-2}, the EDL capacitance increases to 20 mF cm^{-2} when the current density increases from 2 to 20 mA cm^{-2} (geometrical electrode surface) [14,15]. No matter that most of these results are obtained by alternative current (ac) methods they are not "classical" EIS experiments considering a large band of ac frequencies and corresponding equivalent circuit model fitting. Other very important detail in the above-mentioned studies is the maximum H_2SO_4 concentration for which the EDL is studied—it is about 0.05 M, and the electrodes are of "model" type, i.e. PbO_2 electrodeposited on smooth (polished) Pt or Au surface. These conditions are not close to the typical ones for the lead-acid cell—highly porous PbO_2 electrode immersed in 5 M H_2SO_4, frequently with a considerable amount of $PbSO_4$ deposited in the PAM pores when the case of partial state of charge (PSoC) is considered.

The aim of this work is to study the impedance behaviour of the positive plate at different SoC and SoH (state of health) during both the charge and the discharge of the plate, to propose and confirm an equivalent circuit of the positive plate in PSoC and to estimates the dependence of the circuit elements on SoC and SoH.

2. Experimental

The experiments were carried out in three-electrode electrochemical cells consisting of:

- *working electrode*: dry-charged flat positive plate with 3 mm thickness, 8 Ah nominal capacity at 50% PAM utilization, produced by CEAC-EXIDE (France), with grid composition Pb–2.8%Sb. The plates where cut from bigger 40 Ah plates;
- *counter electrode*: two dry-charged CEAC-EXIDE (France) negative plates, with nominal capacity 8 Ah and thickness 3 mm. The plates where also cut from bigger 40 Ah plates;
- *reference electrode*: Ag/Ag_2SO_4 (1.28 s.g. H_2SO_4), +38 mV versus Hg/Hg_2SO_4 in the same solution [16,17].

The electrolyte was H_2SO_4 solution, with a specific gravity (s.g., density) 1.24 g ml^{-1}. The cells were tested on SOLARTRON Multistat 1470 instrument supplied with Frequency Response Analyzer.

After 30 min of soaking in the electrolyte the cells were subjected to a 20 h charge-up at $I = 0.25$ A in order to oxidize the residual quantities of $PbSO_4$ unconverted into PbO_2 or Pb during the formation. After this conditioning of the cells a following cycling regime was applied:

- *Discharge*: $I = -0.8$ A down to $\varphi^+_{cutoff} = 0.75$ V; open circuit 120 min; constant current charge: $I = 0.8$ A up to $\varphi^+_i = 1.38$ V (interruption potential). The pulse current charge was performed with $I = 0.8$ A until a 15% of the nominal capacity was introduced. The applied frequency f and duty cycle $r = ft_{on}$, where the t_{on} is the duration of the charge during one square-wave period, were, respectively $f = 1$ Hz and $r = 1$. After the end of the charge the cell was subjected to 120 min open circuit stay [18].

All impedance measurements were carried out after 120 min open circuit stay in order to be sure that the positive plate has reached steady state conditions. The ac amplitude was 5 mV, keeping the dc potential equal to the one measured in the end of the open circuit stay. The frequency band was between 50 kHz and 0.1 Hz (or lower), with a spectral density of 20 points per decade.

When studying the positive plate impedance in PSoC, the charge or the discharge was interrupted by 2 h open circuit periods for each 1 h of charge or discharge with 0.1 C_{10} rate (0.8 A), at the end of which the EIS was performed. Similar series of experiments were performed also with pulse charge with 0.05 C_{10} rate combining 2 h charge period with 2 h open circuit stay.

Separate experiments with a constant current cycling have been done also in 1.28 s.g. sulphuric acid, after 1 h open circuit stay with ac amplitude 10 mV and 10 points per decade. In the discussion of these results, it will be mentioned specially that they were performed in more concentrated acid.

3. Results and discussion

3.1. Strategy of the analysis of the impedance spectra

In order to analyze the obtained impedance spectra, the following strategy was employed: first the parasitic inductance high frequency "tail" was partially corrected according to the procedure listed below (Section 3.1.1), then a differential impedance analysis (DIA) of the spectra was used in order to recognize the number of the time constants in the system. A brief description of DIA is given in Section 3.1.2. The third step was to propose an equivalent circuit model of the positive plate and to perform a fitting with *Z*-View2 software in order to obtain the values of the equivalent circuit parameters. Using the values of the equivalent circuit parameters, the simulated impedance spectra was subjected to DIA in order to be compared with the DIA data of the experimental spectra. This comparison was used as an addi-

tional validation criterion of the proposed equivalent circuit models.

3.1.1. Correction of the inductance errors in the impedance spectra

The values of the impedance of a lead-acid cell are in the order of few milliohms to few tenths of milliohms or even less, i.e. the impedance is in the lowest range of the used apparatus. The low impedance of the object results in the appearance of very substantial errors in the imaginary part of the spectra due to the parasitic inductance of the cables, current collectors and grids of the plates. In order to reduce the inductance errors we used a procedure developed by Vladikova, Stoynov and Raikova and called "L-correction" [19,20]. According to the procedure, the impedance spectrum of a "dummy" cell with the same configuration of cables and connections as used in the experimental cell is measured, employing the same frequency band and same ac voltage amplitude. In the "dummy" cell, the reference electrode, the counter electrode and the working electrode are short circuited. The dummy cell is considered to be connected in series with the "ideal" experimental cell. Thus the impedance of the "real" cell is a sum of the impedances of the "ideal" cell and the "dummy" cell. In our experiments, the L-correction was partial, because the grids and the active materials inductance were not estimated.

The spectra obtained in 1.28 s.g. H_2SO_4 were not subjected to L-correction.

3.1.2. Differential impedance analysis of the impedance spectra

The DIA is a tool for numerical analysis of the EIS developed recently by Stoynov [21–25] and applied successfully in various electrochemical studies [26–32]. In the DIA, the usual set of impedance data $\{\omega_i, Z'_i, Z''_i\}$ is extended with two more parameters to $\{\omega_i, Z'_i, Z''_i, (dZ'/d\omega)_i, (dZ''/d\omega)_i\}$ where ω is the AC frequency, Z'_i and Z''_i are the real and the imaginary part of the impedance. The derivatives $(dZ'/d\omega)_i$ and $(dZ''/d\omega)_i$ are calculated numerically using a cubic spline interpolation. Using the new data set it is possible to find the frequency distribution of the Local Operating Model (LOM) parameters. The LOM consists of one resistance (additional resistance, R_{add}) in series with a circuit of resistance (effective resistance, R_{eff}) and capacitance (effective capacitance, C_{eff}) in parallel, i.e. LOM represents the model of a simple faradic reaction. The results from DIA can be presented either on so called "temporal plots"—$\log R_{add}(\log \omega)$, $\log R_{eff}(\log \omega)$, $\log C_{eff}(\log \omega)$, or spectral plots $\mathrm{Int}(\log R_{add})$, $\mathrm{Int}(\log R_{eff})$, $\mathrm{Int}(\log C_{eff})$, where Int is the intensity of a given spectral line $\log R_{add}(\omega_i)$. The intensity is the number of points which are in the interval $[\log R_{add}(\omega_i) \pm \delta \log R_{add}]$, $\delta \log R_{add}$ is the spectral density, i.e. the resolution of the method. Our data were analyzed with spectral density of 10 points per decade. Very useful parameter is the time constant of the LOM: $T_{eff} = R_{eff}C_{eff}$. The presence of different non-distributed elements as resistors and capacitors, and corresponding time constants, results in the appearance of plateaus in the temporal plots and peaks in the spectral plots. Thus, without any preliminary information about the properties and structure of the studied system, we can get the values and the number of some or of all of its elements.

3.1.3. Conversion of the constant phase element parameter T into a capacitance

In many cases, when the equivalent circuit approach is applied, some of the capacitive elements in the proposed models are replaced by constant phase element (CPE), which impedance is frequency distributed:

$$Z_{CPE} = T^{-1}(j\omega)^{-P} \quad (1)$$

where $j = (-1)^{1/2}$ is the imaginary unit. When $P = 1$, the CPE is equivalent to a capacitor. The frequency distribution parameter P (the CPE nomenclature is the same as in the Z-View2 software) in the case of capacitive CPE most often represents an anisotropy in the capacitive behaviour of some part of the system (double electric layer, passive layer, etc.). The smaller the value of P, the higher the extent of anisotropy.

The CPE is an empiric parameter and practically the values of T and P are not of great electrochemical significance. In case the CPE is in parallel with a resistor, it can be converted into capacitance according to the relationship proposed recently [33–35]:

$$C_{CPE} = T(\omega''_{min})^{P-1} \quad (2)$$

where ω''_{min} is the frequency corresponding to the local minimum of the $Z''(\omega)$ curve considering the EIS of a resistor in parallel with a CPE circuit only. Using the last equation, the capacitance values were extracted from the CPEs in order to reach to the values of the time constants corresponding to the different phenomena in the positive plate electrochemistry. Since the time constants do not contain information about the size of the system (volume, electrode surface, etc.) they are very convenient when results from many spectra are compared.

3.2. Impedance of the completely charged positive plate

In Fig. 1a, a typical EIS is plotted for a well charged positive plate. The data are L-corrected and the parts, where $Z'' > 0$ were removed. The spectrum was subjected to differential impedance analysis and the obtained temporal plots (logarithm of the module of the LOM parameters versus $\log \omega$) are shown in Fig. 1b. The temporal plot can be divided in two parts. Below 10 Hz the LOM parameters distribution is a smooth function of the frequency with one plateau-like part and low-frequency distributed tail. It is clear that the flat-like parts correspond to a resistor, a capacitor and a time constant. The low-frequency distributed part corresponds to Warburg-type element. According to Stoynov and Vladikova, such type of temporal DIA plots correspond to a capacitor in parallel with a resistor and CPE [21]. The spectral plots of the DIA data, shown in Fig. 1c–e, confirm the presence of non-distributed resistance and capacitance in the system; the values of these elements correspond to the sharp maxima denoted with circles.

Above 10 Hz, the DIA results are quite noisy. The reason should be simple—at high frequencies it seems that $Z'(\omega) \rightarrow R_\Omega$

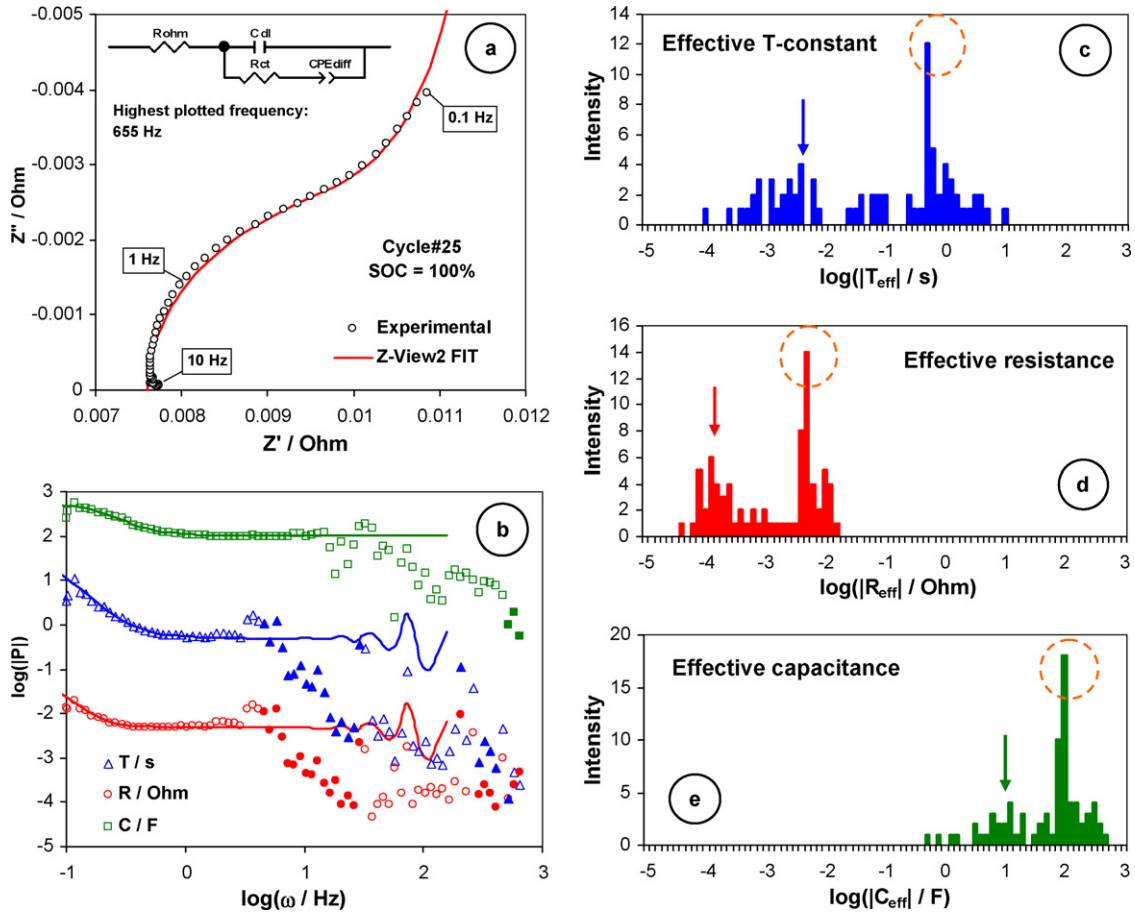

Fig. 1. (a) Electrochemical impedance spectrum of a charged positive plate after 25 charge/discharge cycles. (b) Differenential impedance analysis temporal plot representation of the impedance spectrum, the white-filled symbols correspond to positive values of the LOM parameters, the colour-filled symbols correspond to negative values of the LOM parameters, the solid lines correspond to the DIA of the simulated EIS with the circuit parameters form the best fit. (c–e) Spectral DIA plots of the LOM parameters, the units of the intensity are in number of points per spectral line, the spectral density is 10 points per decade.

and $Z''(\omega) \rightarrow 0$. The ratio signal to noise is also quite low. No matter of this the DIA results are rather strange—in the log (R_{eff}) versus log(ω) there is a distributed part where the values of R_{eff} are negative, followed by plateau-like part where the sign of the R_{eff} is again positive (the symbols corresponding to positive signed LOM parameters are filled with white, the negative values correspond to colour-filled symbols). Since $T_{eff} = R_{eff}C_{eff}$, the effective time constant replays the behaviour of R_{eff}. This result supposes the presence of faster processes in the system with characteristic times of a few milliseconds, proceeding in medium with two orders of magnitude lower resistance (the log R_{eff} is two units lower). The presence of high frequency time constant, resistance and capacitance element can be recognized also in the spectral DIA plots—there is other set of peaks denoted with arrows which are twice smaller and much larger. The recognition of such type of processes regardless of the noise in the system is typical for the method of DIA [24].

The modeling of the low-frequency part of the EIS with an equivalent circuit containing a capacitor in parallel with resistor and CPE, presented in Fig. 1a, is very close to the model proposed by Pavlov and Petkova for a completely charged positive plate and used further to fit data from VRLA cells [36,37]. The resistor R_{ct} stands for the resistance of the charge transfer process during the electrochemical oxidation of the $PbSO_4$ to PbO_2. The CPE representing the EDL capacitance in the work of Pavlov and Petkova is replaced here by the capacitor C_{dl}. The distributed element CPE_{diff} describes the diffusion of the electroplyte. Considering the high porosity and surface area of the PAM, the exponent "P" in CPE_{diff} can be quite different from the value of 0.5, which is typical for the Warburg element. The resistor R_{Ω} (denoted also as R_{Ω} in the equivalent circuits) in series accounts the resistance of the electrolyte and the solid-state parts of the cell (wires, current collectors, grids, positive active material non-participating in the electrochemical processes etc.). The equivalent circuit and the result from the fit are presented in Fig. 1a. Using the model parameters, a simulated impedance spectrum was obtained. The simulated data were subjected to DIA and the comparison between the experimental and simulated temporal plots are presented in Fig. 1b. In the low-frequency part of the temporal plot, where the experimental data are non-scattered the coincidence between simulated and experimental results is excellent. In the high frequency part the difference is obvious. At about 100 Hz, the simulated values of T_{eff} and R_{eff} begin to oscillate, because the accuracy of the simulated data is five digits (Z-View2 software). The observed

Table 1
Results of the Z-View equivalent circuit fitting of the EIS of a completely charged and completely discharged positive plate

Element	Charged positive plate	Discharged positive plate
R_Ω (Ω)	7.6	14.9
R_{ct} (mΩ)	4.7	8.4
$CPE_{diff} - T$ (Ω^{-1})	384	50.1
$CPE_{diff} - P$	0.89	0.70
C_{dl} (F)	104	24.7
$CPE_{ic} - T$ (Ω^{-1})	n.a.	8.98
$CPE_{ic} - P$	n.a.	0.40
R_{ic} (mΩ)	n.a.	15.7

difference confirms the existence of an additional processes in PAM. The results of the Z-View fit are listed in Table 1.

3.3. Impedance of the completely discharged positive plate

The impedance spectrum of a completely discharged positive plate is plotted in Fig. 2a. The data were analyzed by DIA and the corresponding temporal plots of the LOM parameters distribution are shown in Fig. 2b. The obtained $\log T_{eff}$ versus $\log \omega$ dependence features constant slope close to the unit, which is confirmed also in its spectral form, shown in Fig. 2c. Such type of behaviour of T_{eff} supposes the presence of more than one distributed element in the equivalent circuit of the positive plate. In the temporal plot of the C_{eff}, a plateau-like zone is not observable, but there are two zones with different slopes. The spectral plot of the C_{eff} shown in Fig. 2e is similar to the efficient time constant spectral plot—there are no well pronounced spectral lines. In the spectral plot of the effective resistance there is one well pronounced spectral line, which lays close to the higher peak in Fig. 1d. As a whole, the temporal plots of T_{eff}, R_{eff} and C_{eff} are smooth almost within five frequency decades. This indicates the existence of at least two circuits. According to the model proposed by Pavlov and Petkova [36] for the equivalent circuit of the discharged positive plate, a circuit of resistor and CPE in parallel should be added in series to the circuit accounting the impedance of the electrochemical reaction of $PbSO_4$ oxidation. The combination of resistor (denoted as R_{ic}) and capacitive CPE (denoted as CPE_{ic}) describes the resistance and the dielectric properties of a partially discharged corrosion layer (CL) and active mass collecting layer (AMCL), which are result from the formation of low conductive species like $PbSO_4$, PbO_n ($n < 1.6$) and PbO. Thus the EIS data were fitted using the model shown in Fig. 2a. The only difference between this model and the previously proposed by Pavlov and Petkova is the description of the EDL capacitance with a capacitor. The modified model fits the

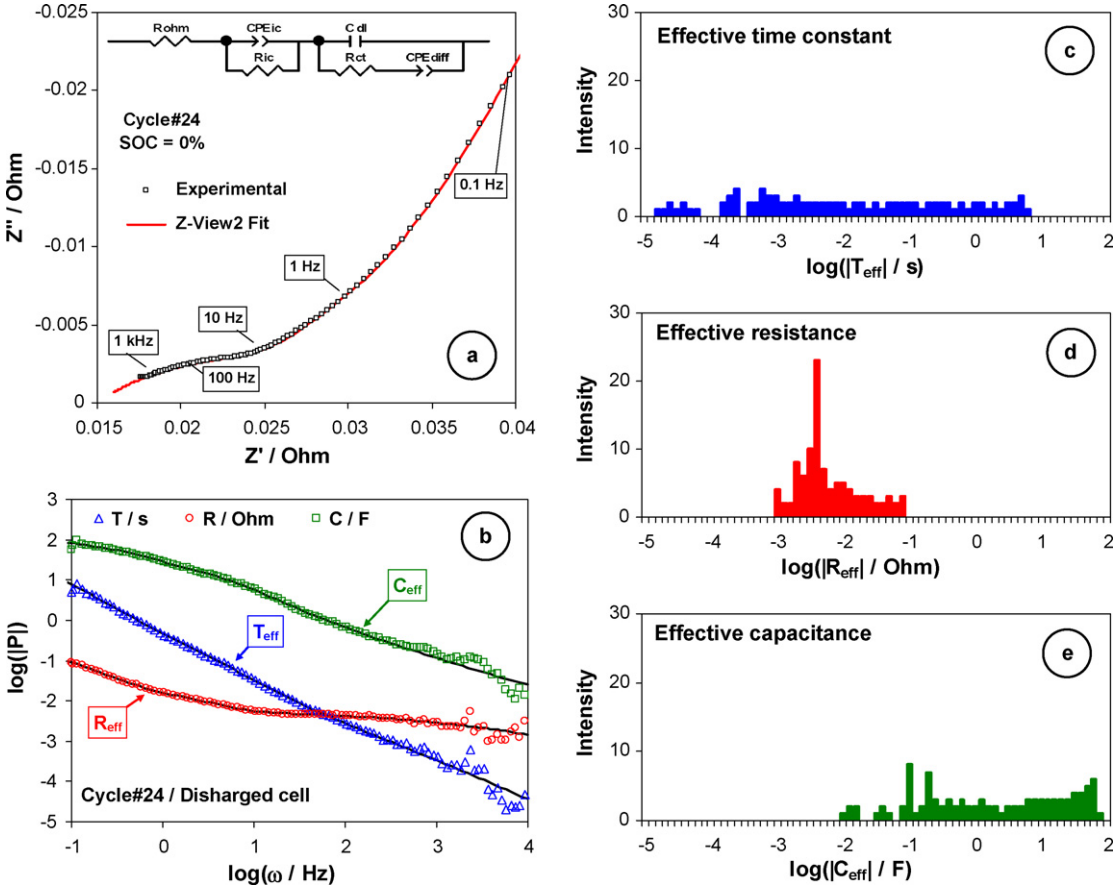

Fig. 2. (a) Electrochemical impedance spectrum of a discharged positive plate after 24 charge/discharge cycles. (b) Differential impedance analysis temporal plot representation of the impedance spectrum, the solid lines correspond to the DIA of the simulated EIS with the circuit parameters form the best fit. (c–e) Spectral DIA plots of the LOM parameters, the units of the intensity are in number of points per spectral line, the spectral density is 10 points per decade.

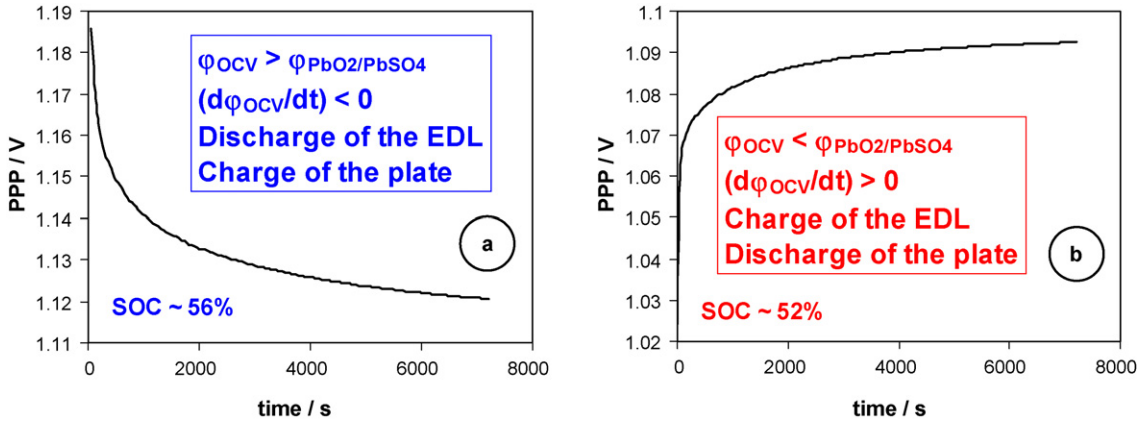

Fig. 3. Positive plate potential (PPP) open circuit transients at partial state of charge during the charge (a) and the discharge (b).

experimental data well. A perfect match between the simulated and the experimental DIA temporal plots was obtained too. The results from the fit are listed in Table 1.

3.4. Impedance of the positive plate in partial state of charge

3.4.1. Processes on the positive plate during the open circuit stay period in PSoC

During the open circuit the current flowing through the cell is apparently equal to zero. Regardless of this fact, there are electrochemical process taking place both on the positive and on the negative plate such as corrosion and self-discharge. These processes proceed with different rates. Here, the processes which are of particular interest are the fastest processes taking place immediately after switching off the current. The open circuit transients for half-charged and half-discharged positive plate are shown in Fig. 3a and b. It is obvious that the positive plate potential hardly reach a steady state value within 2 h. During this period the main energy dissipation mechanism is the self-discharge (Fig. 3a) or the self-recharge (Fig. 3b) of the EDL [38,39]. The self-discharge/charge of the EDL is lumped with the corresponding electrochemical processes—$PbSO_4$ oxidation and O_2 evolution (Fig. 3a) or PbO_2 reduction (Fig. 3b). Thus, regardless of the zero net current in the system, during the open circuit period we have electrochemical reactions which proceed in defined direction, i.e. when the charge current is switched off the charge reaction continues due to the energy stored in EDL and vice versa, when the discharge current is switched off the formation of $PbSO_4$ continues because of the recharge of the EDL. A detailed discussion on this topic has been done in the first part of this work [1]. Therefore the analysis of the impedance spectrum of the positive plate will be done for two main cases—for PSoC during the charge and during the discharge.

3.4.2. Impedance of the positive plate in PSoC during the charge

The impedance spectrum of the positive plate at SOC = 34% during a charge with pulse current after 23 charge/discharge cycles is plotted in Fig. 4a. The Nyquist plot can be divided into three parts—between 500 and 41 Hz there is a part of a capacitive semi-circle, followed by a well pronounced pseudo-inductive semi-circle and between 3.3 and 0.1 Hz a $Z''(Z')$ dependence typical for a charged plate can be observed. The obtained spectra for PSoC differ substantially both from the impedance spectrum in completely charged and completely discharged positive plates. The DIA temporal plot corresponding to the EIS at SOC = 34% is shown in Fig. 4b. Three frequency domains are clearly distinguished. The low-frequency domain is very similar to the DIA temporal plot of the plate at SOC = 100%. It is clear that it corresponds to the electrochemical reaction of the $PbSO_4$ oxidation. The mean-frequency domain corresponds to the pseudo-inductive loop in the Nyquist plot. It contains one negative resistance element and one negative capacitance element, giving together a positive time constant. Such result indicates the presence of adsorption processes or passivation-type chemical reactions on the lead dioxide surface. These processes are two orders of magnitude faster than the charge transfer process. The high frequency domain corresponds to a RC-circuit with a time constant 3–4 orders of magnitude faster than the charge transfer during the electrochemical reaction. Considering the fact that the charge transfer of the $PbSO_4$ is much facilitated, a process which is 1000 times faster should correspond to the charge transfer of the much smaller species—obviously electrons in a medium with high conductance. These three frequency domains give three groups of peaks in the DIA spectral plots. Especially the peaks of the R_{eff} and C_{eff} are very well pronounced.

In order to propose an adequate equivalent circuit model of the positive plate in partial state of charge we have to take a look at the mechanism of the lead dioxide formation and the structure of the positive active material in the lead-acid battery. Considering the gel-crystal model of the lead dioxide, the particles building the positive active material consist of crystalline core of α- or β-PbO_2 while the surface, which is in contact with the H_2SO_4 solution, is hydrated [40–49]. The hydrated parts consist of hydrated polymer chains of lead dioxide, denoted as $PbO(OH)_2$ (along these chains electrons ensure the electric connection between the electrolyte and the crystalline lead dioxide). The conductivity of the hydrated layer is strongly limited by the degree of the hydration, i.e. by the water content in the dioxide. According to the gel-crystal model, the mechanism of the

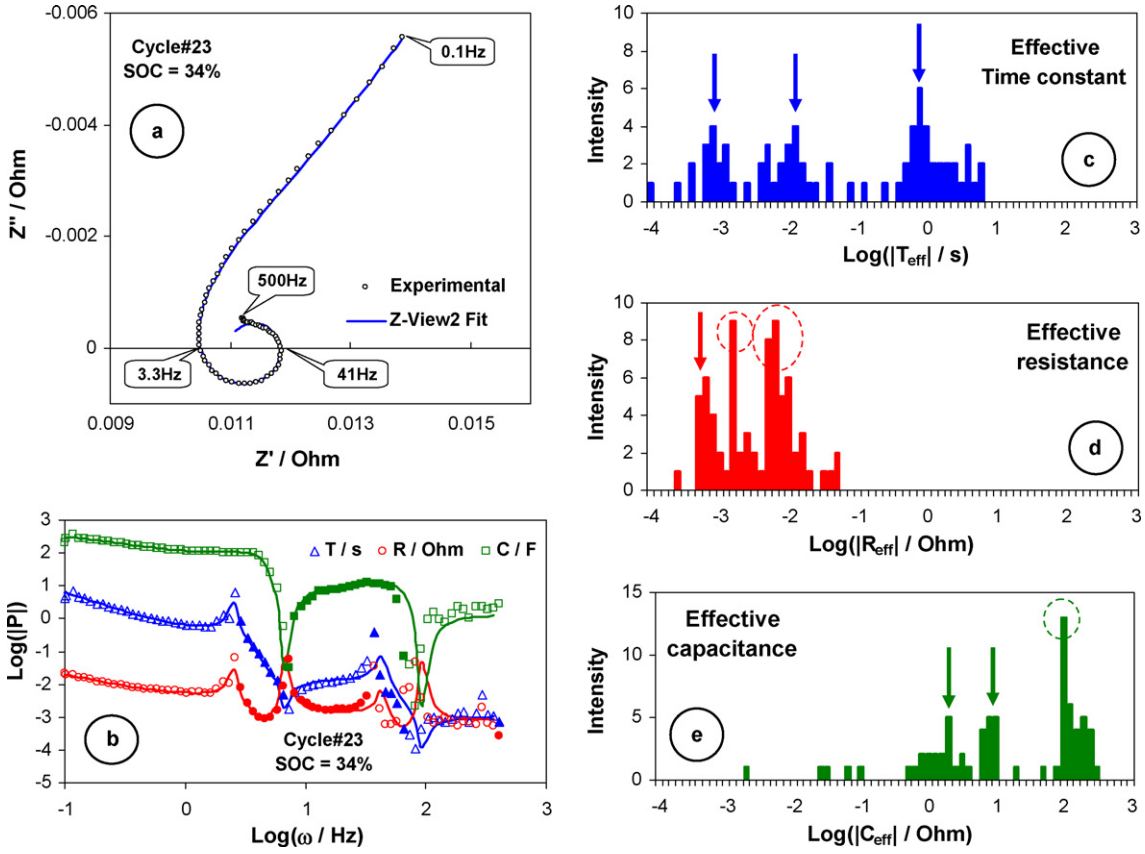

Fig. 4. (a) Electrochemical impedance spectrum of a partially charged positive plate after 23 charge/discharge cycles in 1.24 s.g. electrolyte, SoC = 34%. (b) Differential impedance analysis temporal plot representation of the impedance spectrum, the white-filled symbols correspond to positive values of the LOM parameters, the colour-filled symbols correspond to negative values of the LOM parameters, the solid lines correspond to the DIA of the simulated EIS with the circuit parameters form the best fit. (c–e) Spectral DIA plots of the LOM parameters, the units of the intensity are in number of points per spectral line, the spectral density is 10 points per decade.

$PbSO_4$ oxidation can be represented by the following reactions:

$$PbSO_4{}^{(crystal)} \Leftrightarrow Pb^{2+} + SO_4{}^{2-} \quad (3a)$$

$$Pb^{2+} \rightarrow Pb^{4+} + 2e^- \quad (3b)$$

$$Pb^{4+} + 4H_2O \rightarrow Pb(OH)_4{}^{(colloid)} + 4H^+ \quad (3c)$$

$$Pb(OH)_4{}^{(colloid)} \rightarrow PbO(OH)_2{}^{(gel\ PbO_2)} + H_2O \quad (3d)$$

$$PbO(OH)_2{}^{(gel\ PbO_2)} \Leftrightarrow \beta\text{-}PbO_2{}^{(crystal)} + H_2O \quad (3e)$$

The Pb^{2+} ions, dissolved form the $PbSO_4$ crystals, are oxidized on the surface or in the volume of the gel part of the PbO_2. The latter consists of hydrated polymer chains of lead dioxide, denoted as $PbO(OH)_2{}^{(gel\ PbO_2)}$. The electrochemical reaction (3b) proceeds on determined active centers—these are the places in the hydrated lead dioxide where both electronic and ionic conductance is maximal. Since the Pb^{4+} ions are unstable in water solutions, they react fast with water giving a colloid solution of $Pb(OH)_4$ (Reaction (3c)). The latter dehydrates partially to hydrated lead dioxide (Reaction (3d)). The hydrated lead dioxide is in dynamic equilibrium with the one in crystalline state (Reaction (3e)).

The $PbSO_4$ is dielectric medium and its solubility depends only on the H_2SO_4 concentration. Thus the contribution of the Reaction (3a) process will be represented in the Wartburg-type CPE_{diff} which is included in the electrochemical reaction circuit (Figs. 1a, 2a and 5). The Reaction (3b) is a charge transfer process and it can be described with a combination of resistance and capacitance in parallel—R_{ct} and C_{dl}. This explains the origin of the low-frequency domain in the EIS in PSoC, which is typical both for a completely charged and completely discharged positive plate.

The Reactions (3c)–(3e) are chemical processes, i.e. there is no charge transfer. The PAM is a porous system, with conditions suitable for the development of membrane phenomena which can lead to an alkalization in the smallest pores, where the ionic diffusion is hindered [50]. The local alkalization can decrease the rate of the $Pb(OH)_4$ dehydration (Reaction (3d)), which is equivalent to a passivation process because the $Pb(OH)_4$ possesses much higher ohmic resistance than $PbO(OH)_2$ and β-PbO_2 species. Thus the presence of a pseudo-inductive loop can be explained by a slower dehydration of the $Pb(OH)_4$ in the micro and sub-micro pores of PAM. The possibility that the passivation can be caused by $PbSO_4$ crystals can be firmly rejected because such type of pseudo-inductive loop is never observed in completely discharged state and is rather untypical for partially discharged plates (see the following section). The current meaning of the term “passivation” should be divided

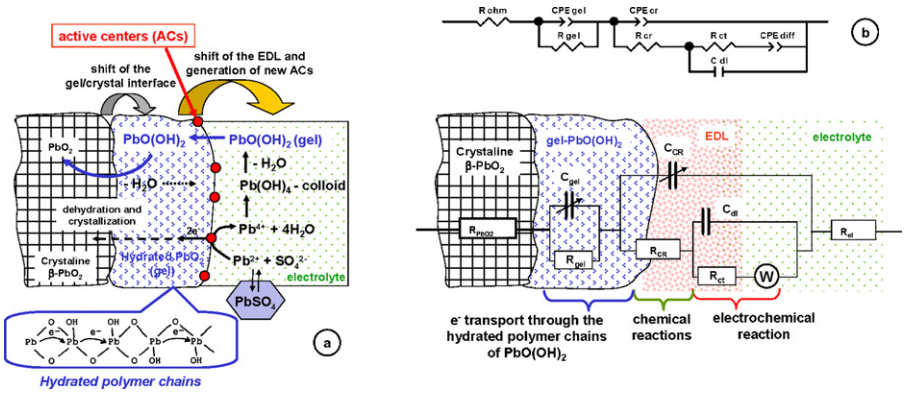

Fig. 5. Scheme of the PbO_2/electrolyte interface, the reactions taking place there (a) and their equivalent circuit representation during the charge of the positive plate (b).

from its "classical" use in the corrosion science describing the formation passive layers with resistance few orders of magnitude higher than the resistance of the supporting phase. Even denoted as passivation, the DIA results show that the process of $Pb(OH)_4$ dehydration is much faster than the electrochemical reaction (3b).

The low time constant of the high frequency loop in the EIS of a partially charged positive plate supposes that its corresponding process involves species smaller than the ions in the electrolyte solution in the pores. In discharged state such high frequency loop is associated with the electronic transport through the partially discharged interface (CL + AMCL) [36,37]. But this resistance in PSoC is much lower: 1–2 mΩ (or less) versus 15–20 mΩ in completely discharged state. The other medium in PAM, uniting both electrical and dielectrical properties is the hydrated part of the lead dioxide $PbO(OH)_2$: increasing the hydration both the resistance and the capacitance of the gel will increase, and vice versa. The mechanism of the electronic conductance in the gel part of the lead dioxide is similar to this in the conducting polymers.

Uniting the information from DIA (Fig. 4b–e) and the gel-crystal model of the lead dioxide (Fig. 5a), the model shown in Fig. 5b was used to fit the experimental data for the EIS in PSoC. An important question considering this model is the joint circuit representation of the electrochemical and the chemical reactions. Two arrangements are possible—the first one is shown in Fig. 5b, and the second one is to arrange all three circuits in series, i.e. a classical representation of a consecutive processes. The DIA plots of the simulated spectra with both equivalent circuit arrangements were almost identical and also match well with the DIA results of the experimental spectra. The results from the *Z*-View fitting about the sum of the least complex squares and the corresponding normalized sum show that the fitting with the model from Fig. 5b results in values about 5% less than fitting with the alternative model, i.e. the statistics shows that the first model is 5% "better". In general these 5% are a too small value to be used as a reliable criterion to accept or reject one of the two models (the value varies between 1 and 10% for different values of the SoC). But there is another explanation why the model shown in Fig. 5b is more relevant—the proposed model supposes direct relation and feedback between the chemical and the electrochemical process: the electrode surface is build by the chemical reactions, which are results form the electrochemical reaction taking place on the same electrode surface. In a series connection between all circuits (in the alternative model) such type of direct relation and feedback in not obvious.

3.4.3. *Impedance of the positive plate in PSoC during the discharge in 1.24 s.g. H_2SO_4*

The impedance spectrum of the positive plate at SOC = 40% (versus the nominal 8 Ah capacity) during a discharge with $0.1C_{10}$ constant current (2 h discharge followed by 2 h open circuit stay) after 5 charge/discharge cycles in sulphuric acid with s.g. 1.24 is plotted in Fig. 6a. The absence of a pseudo-inductive loop is typical for the EIS of the partially discharged positive plate cycled in this slightly diluted acid. The DIA temporal plot can be divided in two parts—the low-frequency part ($\omega < 10$ Hz) coincides well with the results obtained for a well charged plate. It can be connected with the electrochemical reaction of reduction of Pb(IV) to Pb(II). The high frequency part is similar to the high frequency capacitive part observed in the EIS results of partially charged positive plate. It is obvious that this high frequency loop is due to the transfer of the electrons through the gel part of the lead dioxide. This consideration can be confirmed by the DIA spectral plots, where a pair of peaks was observed in the spectra of the T_{eff}, R_{eff} and C_{eff}. Thus the equivalent circuit, modelling the partially charged plate, should be used, setting the impedance of the elements corresponding to the chemical reactions equal to zero. The results from the fit are listed in Table 2. The DIA temporal plots of the experimental and the simulated data are compared in Fig. 6b. It can be seen that the model matches the experimental data quantitatively.

3.4.4. *Impedance of the positive plate in PSoC during the discharge in 1.28 s.g. H_2SO_4*

The impedance spectrum of the positive plate at SOC = 51% during an interrupted discharge with $0.1C_{10}$ constant current (1 h discharge followed by 1 h open circuit stay) after 10 charge/discharge cycles in sulphuric acid electrolyte with specific gravity 1.28 g ml^{-1} is plotted in Fig. 7a. The obtained result is very similar to the picture observed during the partial

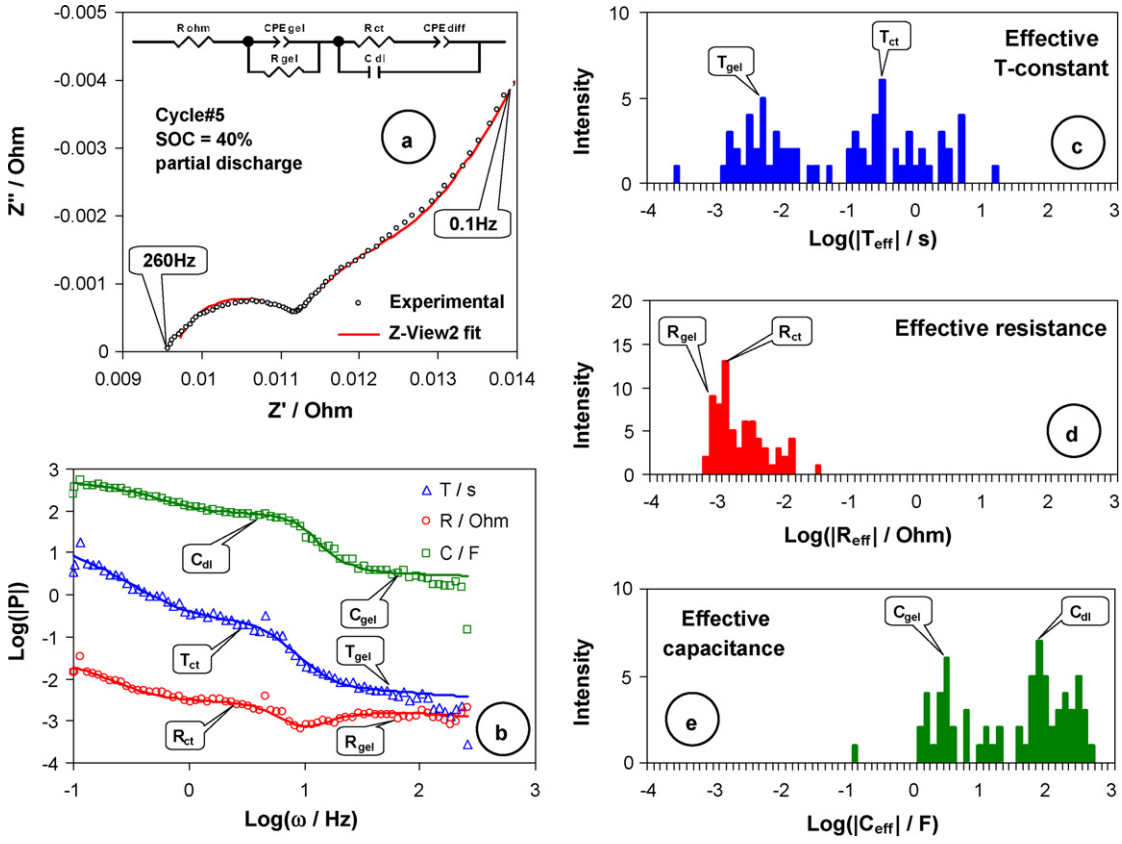

Fig. 6. (a) Electrochemical impedance spectrum of a partially discharged positive plate after 5 charge/discharge cycles in 1.24 s.g. H_2SO_4, SoC = 40%. (b) Differential impedance analysis temporal plot representation of the impedance spectrum, the solid lines correspond to the DIA of the simulated EIS with the circuit parameters form the best fit. (c–e) Spectral DIA plots of the LOM parameters, the units of the intensity are in number of points per spectral line, the spectral density is 10 points per decade.

charge of the positive plate. The DIA data also confirm this conclusion. The appearance of a pseudo-inductive loop in the Nyquist plot clearly shows the proceeding of chemical processes in the mechanism of the positive plate discharge. According to the gel-crystal model of the lead dioxide the mechanism of the discharge of the positive plate can be presented as follows [40–42,44,51,52]:

$$\beta\text{-}PbO_2{}^{(crystal)} + H_2O \Leftrightarrow PbO(OH)_2{}^{(gel\,PbO_2)} \quad (4a)$$

$$PbO(OH)_2 + 2H^+ + 2e^- \rightarrow Pb(OH)_2 + H_2O \quad (4b)$$

$$Pb(OH)_2 + 2H^+ \rightarrow Pb^{2+}H_2O \quad (4c)$$

$$Pb^{2+} + SO_4{}^{2-} \Leftrightarrow PbSO_4 \quad (4d)$$

The electrochemical reaction (4b) proceeds by "solid sate" type mechanism where the protons diffuse from the electrolyte through the gel part of the lead dioxide towards the active centres and the electrons are transported along the hydrated polymer chains. The produced water molecules hydrate further the crystalline part of the lead dioxide (Reaction (4a)). The formed $Pb(OH)_2$ can be neutralized by more protons coming from the

Table 2

Element	Partially charged positive plate (H_2SO_4—1.24 s.g., 23 cycles)	Partially discharged positive plate (H_2SO_4—1.24 s.g., 5 cycles)	Partially discharged positive plate (H_2SO_4—1.28 s.g., 10 cycles)
R_Ω (mΩ)	11.1	9.69	8.98
R_{ct} (mΩ)	3.74	2.47	<0.1
$CPE_{diff} - T$ (Ω^{-1})	200.7	306.6	285.2
$CPE_{diff} - P$	0.68	0.75	0.45
C_{dl} (F)	127.1	85.92	263
$CPE_{gel} - T$ (Ω^{-1})	1.474	4.094	3.022
$CPE_{gel} - P$	1	0.95	1
R_{gel} (mΩ)	1.04	1.55	0.75
$CPE_{cr} - T$ (Ω^{-1})	−13.32	n.a.	−22.96
$CPE_{cr} - P$	1	n.a.	1
R_{cr} (mΩ)	−1.43	n.a.	−0.48

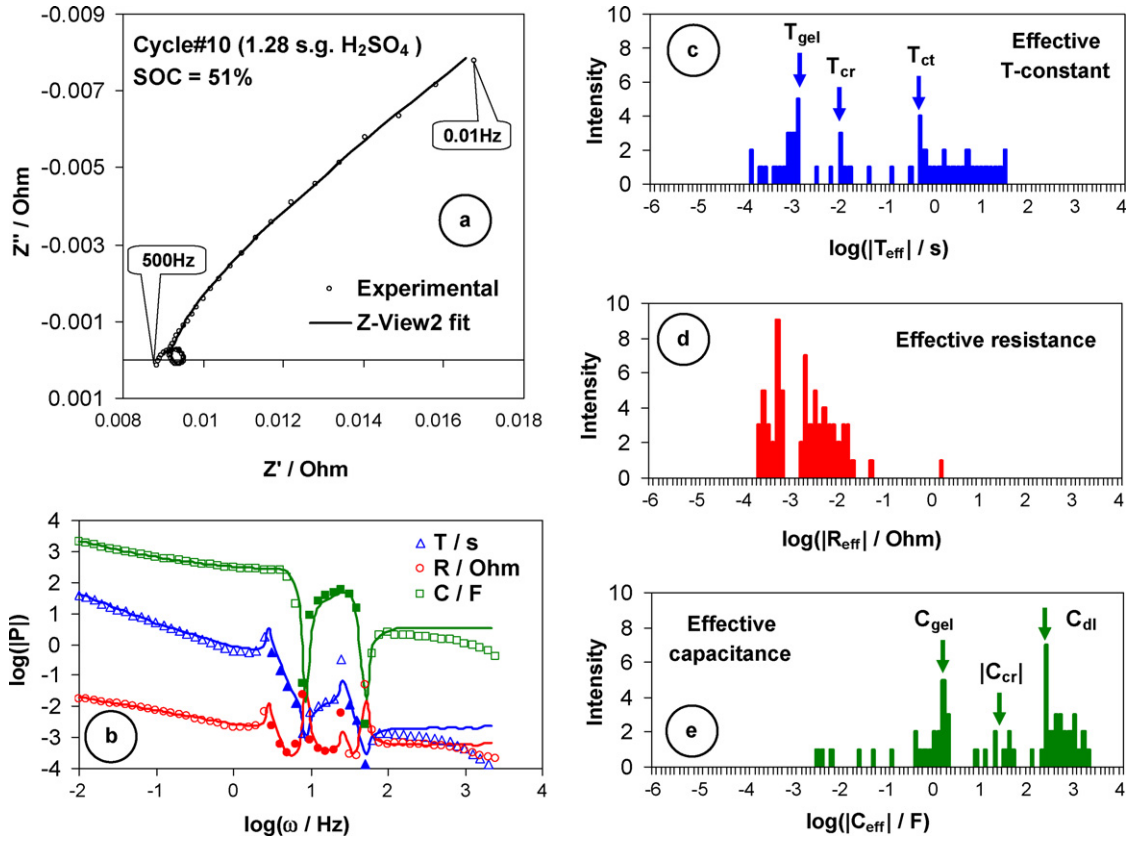

Fig. 7. (a) Electrochemical impedance spectrum of a partially discharged positive plate after 10 charge/discharge cycles in 1.28 s.g. H_2SO_4, SoC = 51%. (b) Differential impedance analysis temporal plot representation of the impedance spectrum, the white-filled symbols correspond to positive values of the LOM parameters, the colour-filled symbols correspond to negative values of the LOM parameters, the solid lines correspond to the DIA of the simulated EIS with the circuit parameters form the best fit. (c–e) Spectral DIA plots of the LOM parameters, the units of the intensity are in number of points per spectral line, the spectral density is 10 points per decade.

electrolyte or can decompose to orthorhombic-PbO [41] and water. The last processes are the diffusion of Pb^{2+} towards the volume of the PAM pores and precipitation of $PbSO_4$. Since the ohmic resistance of the $Pb(OH)_2$ and orthorhombic-PbO is quite high, the electrochemical process (4b) leads to a passivation of the PAM surface and, respectively the dissolution of these species in the reaction (4c) is a depassivation process. The appearance of the pseudo-inductive loop indicates that the depassivation process is slowed down in more concentrated acid.

This result coincides with some recently reported results about the electrochemical activity of the lead dioxide in electrolytes with different concentrations. Both the studies on flat model electrodes and on pasted positive plates show that electrolyte density equal to 1.28 s.g. or higher causes loss of electrochemical activity of the lead dioxide [53–55] as well as decreased discharge capacity and shorter cycle life of the positive plate [56].

A scheme of the reactions during the discharge of the positive plate is presented in Fig. 8. This reaction scheme is similar to, but not the same as the one considering the charge of the positive plate (Fig. 5a). Therefore in order to fit the spectra obtained in 1.28 s.g. H_2SO_4 the equivalent circuit shown in Fig. 5b was used. The results from the fit are presented in Table 2. An interesting result here was the value of the charge transfer resistance—during the whole discharge it was not possible to obtain adequate value of this parameter: the *Z*-View2 fitting procedure gave usually extremely small numbers $\sim 10^{-10}$ Ω, which means that the charge transfer is very facilitated. The fitting

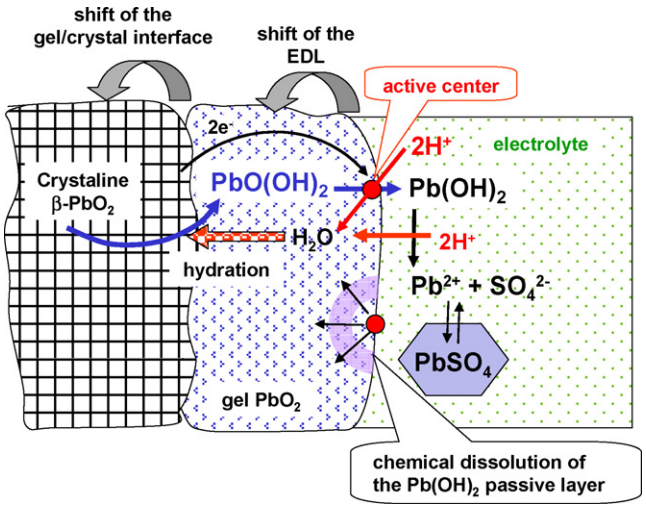

Fig. 8. Scheme of the PbO_2/electrolyte interface and the reactions taking place there during the discharge of the positive plate.

was performed with fixed values about 50–100 μΩ. The value of the R_{ct} was also hardly observable even in the DIA temporal plot of the effective resistance (Fig. 7b), because there is no flat part of the $\log R_{eff}(\log \omega)$ curve in the region between the low-frequency distributed diffusion domain and the domain corresponding to the negative resistance of the chemical reactions. It is due to the presence of the pseudo-inductive time constant, which "hides" the flat high frequency branch of the R_{eff} corresponding to the electrochemical reaction. But even with fixed values of R_{ct}, the model fits well the experimental data. The high frequency discrepancy in the DIA temporal plots (Fig. 7b) between the experimental and simulated results can be related to the presence of higher inductance error, which was not corrected in the spectra obtained in the more concentrated electrolyte. The presence of the three time constants is clearly observable in the spectral plots of the effective time constant and the effective capacitance of the system.

3.5. Evolution of the equivalent circuit parameters during the charge and the discharge of the positive plate

The evolution of the equivalent circuit parameters during the charge and the discharge reveals important information about the mechanisms of the charge and discharge process. It can help also in the development of more advanced methods for state of charge and state of health estimation considering the concept of lead-acid cells/batteries with integrated reference electrode(s) proposed recently by Ruetschi [16,17,57].

Using the differential impedance analysis approach it is possible to establish the local efficient capacity C_{eff}, efficient resistance R_{eff} and additional resistance R_{add} from very little number of points from the impedance spectra, taken in a narrow frequency domain (one decade for example). In our case this number of points is four, since the cubic spline used in the differentiation procedure uses a four-point interpolation scheme, but it can be restricted to three points or expanded to five. The increase of the number of frequencies in a commercial SoC/SoH impedance-base measuring device will increase its price and accuracy and vice-versa. The DIA results show that the choice of frequency domain corresponds very well to a choice of RC-circuit in the positive plate model. Thus if the DIA temporal plots are nearly flat in this frequency domain, the values of C_{eff}, R_{eff} and R_{add} will be very close to the model parameters C, R and R_Ω from some of the circuits constituting the model of the positive plate. So, knowing which parameter is sensitive to SoC/SoH, and which frequency domain is characteristic for the chosen RC-circuit, DIA becomes an efficient tool for SoC/SoH estimation. For example, the price and the size of such kind of tool can be much lower compared to a frequency response analyzer, providing more accurate but similar information, after an equivalent circuit fitting.

3.5.1. Evolution of the ohmic resistance R_Ω (R_{ohm})

The ohmic resistance represents the sum of the resistances of the conducting elements in the cell. These are the cables, the current collectors, the grids and also the electrolyte and the parts of PAM which do not participate in this moment in the electrochemical reactions but which conduct the electrons form the reaction sites to the lead grid. Thus the parameter R_Ω depends on two dynamic "elements"—the electrolyte, because the H_2SO_4 is the third active material, and the PbO_2 skeleton together with PAM/grid interface changes, due to electrochemical and chemical reactions like partial charge/discharge, hydration/dehydration, corrosion etc. A typical dependence of the ohmic resistance on SoC for one charge/discharge cycle is shown in Fig. 9, for different cells (but with identical plates and electrolyte relative density) after 5 and after 72 cycles. The state of charge is referred to previously measured the discharge capacity (without interruptions).

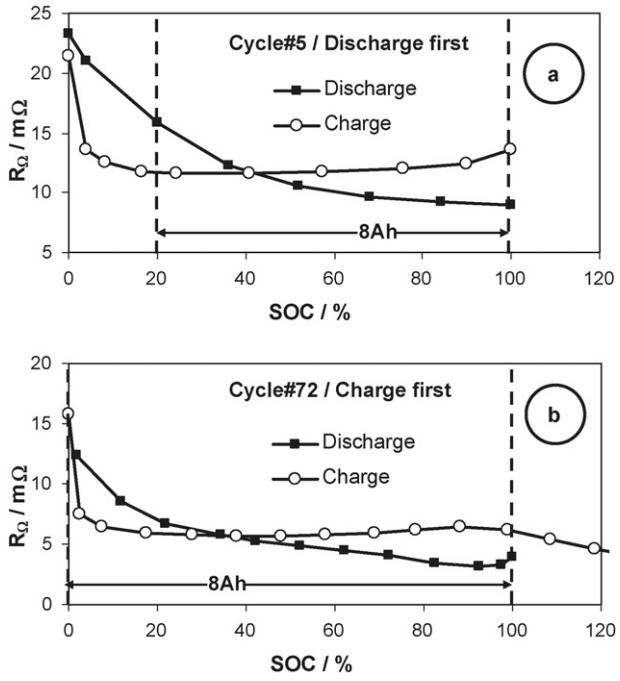

Fig. 9. Dependence of the ohmic resistance R_Ω on state of charge for a cell subjected to 5 cycles (a) and for a cell subjected to 72 cycles (b) with 100% DOD at 10 h rate of the charge and the discharge (0.8 A).

The zone where the nominal capacity (8 Ah) is discharged is shown on both plots of Fig. 9. The results obtained after 5 and 72 cycles are very similar. There is substantial difference between the curves of R_Ω(SoC) obtained during the charge and the discharge. In both cases the dependence is strongly non-linear. During the discharge, R_Ω increases monotonously. Similar result is reported by Huet et al. for the R_{HF} of the battery—the real part of the impedance at fixed high frequency (HF), for which the imaginary part is zero or close to it [58]. R_{HF} is close to the internal resistance of the battery. The behaviour of R_Ω during the charge is rather unexpected. In the beginning of the charge, R_Ω decreases abruptly and after this it remains almost constant for the whole charge. It clearly demonstrates that the nature of this parameter is quite complicated and it is not very suitable for estimation of the SoC. The difference between the curves for the charge and the discharge reflects the difference in the mechanisms of the charge and the discharge (they are not simply the same electrochemical reactions taking place in opposite directions).

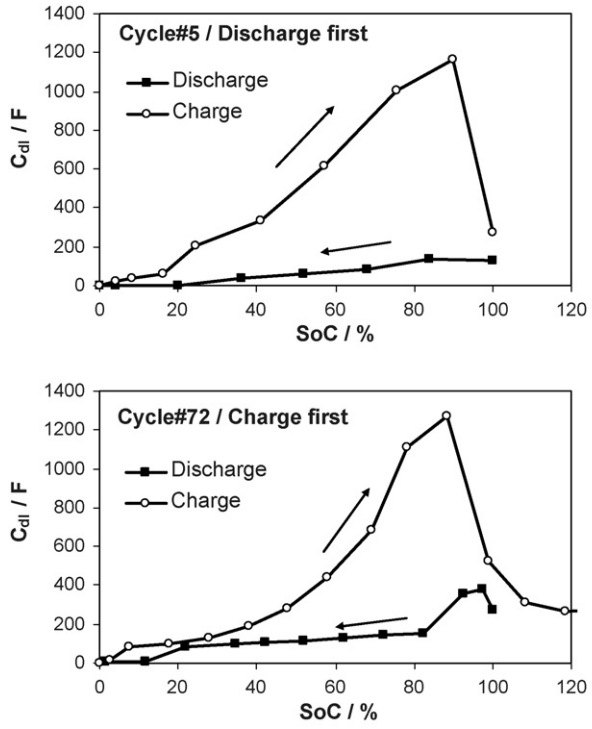

Fig. 10. Dependence of the EDL capacitance C_{dl} on state of charge for a cell subjected to 5 cycles and for a cell subjected to 72 cycles with 100% DOD at 10 h rate of the charge and the discharge (0.8 A).

3.5.2. Evolution of the double layer capacitance C_{dl} and structure of the double layer on the surface of the hydrated lead dioxide

The evolution of the double layer capacitance C_{dl} for the EIS series commented in the previous section is shown in Fig. 10. It can be seen that the dependence of C_{dl} on SOC remains almost the same with ageing of the positive plate (it should be mentioned that regardless of the big cycle number, 72 cycles, the capacity of the plate was very close to its nominal value, i.e. the state of health was still very high). But much more interesting fact is the observed huge hysteresis between the data during the charge and the discharge. This hysteresis was observed at both electrolyte densities (1.24 and 1.28 g ml^{-1}). In all the cases the C_{dl} values during the charge were about 5–6 times higher than the corresponding values during the discharge. Practically this hysteresis makes the use of C_{dl} of the positive plate hardly applicable as a good state of charge estimation criterion. The value of the EDL capacitance is nearly proportional to the electrode surface and hence to the state of health of the positive plate. This statement is in agreement with the obtained results for SoC value between 0 and 80–90% both for the charge and the discharge. On the other hand the surface of the lead dioxide during the charge and during the discharge at fixed SoC should be approximately the same during the considered charge/discharged cycle. That's why the reason leading to the observed hysteresis should be connected with changes in the structure of the double layer due to the electrochemical and chemical processes during the discharge, the charge and the overcharge of the positive plate.

The usual values of the electrolyte concentration in a completely discharged lead-acid cell can vary depending on the cell design, but it is normally above 1–2 M (s.g. 1.06–1.12 g ml^{-1}). Thus, even in discharged state, the double layer on positive plate has a Helmholtz structure, i.e. there is no diffuse part in the volume of the electrolyte. The main part of the sulphuric acid is dissociated to H^+ and HSO_4^-, where most of the H^+ ions are solvated by few water molecules, while the HSO_4^- ions are almost non-solvated. The surface of the lead dioxide is hydrated and the HSO_4^- ions build a Stern layer in the EDL, due to their chemisorption there. Similar EDL model of metal hydroxide is discussed in details recently by Hiemstra and Van Riemsdijk [59]. In a case like this the dielectric constant ε_1, which stays in the equation for the capacitance of plain-parallel capacitor $C = \varepsilon_1 \varepsilon_0 d^{-1}$ (d: EDL thickness; $\varepsilon_0 = 8.85 \times 10^{-12}$ F m^{-1}) will have a value close to the dielectric constant of the "volume" electrolyte, i.e. about 80 and the EDL capacitance will be about 1 F m^{-2}. This model of the EDL during the charge is presented in Fig. 11a.

When the SoC of the positive plate exceeds 75% the process of oxygen evolution starts in parallel with the main reaction:

$$2H_2O \rightarrow O_2 + 4H^+ + 4e^- \quad (5)$$

The result is a production of non-solvated H^+ in the Stern layer. These H^+ ions remain there held either by adsorption on the electrode surface or by formation of ionic couples with the HSO_4^- ions. The absence of sphere of solvating H_2O molecules around the H^+ ions makes them strongly fixed to the electrode surface. The incorporation of H^+ ions in the Stern layer will decrease the density of the surface charge in EDL and hence its electrostatic capacitance. This explains why the C_{dl} versus SoC dependence passes a maximum at about 80–90% SoC. The corresponding structure of the EDL is shown in Fig. 11b.

The first step of the discharge of the positive plate results in formation of water molecules due to the reaction between the $Pb(OH)_2$ and H^+ (Eq. (4b)). The water molecules are formed between the Stern layer and the electrode surface. Thus during the discharge the structure of the double layer will be similar to the structure of the EDL on the metal surfaces. It is shown in Fig. 11c.

The water molecules remain connected to the electrode surface due to formation of coordination bonds with the lead dioxide surface (chemisorption of water). Such kind of water monolayer is specifically ordered and its dielectric constant ε_2 is markedly lower than the "volume" electrolyte [60]. A typical value of ε_2 is about 6. This structure of EDL is typical for the metal surfaces and can be represented by two capacitors in series (Fig. 11c). Here the surface density of the charge is close to the one during charging before the start of the oxygen evolution. The EDL form Fig. 11c will have capacitance about 5–6 times lower than in Fig. 11a at the same surface density of the charge. Thus combining the gel-crystal model of Pavlov with the recent theories about the structure of the EDL on the surface of metal hydroxides, the hysteresis in the C_{dl} versus SoC curves can be explained.

3.5.3. Evolution of the charge transfer resistance R_{ct}

This parameter is associated with the rate of the two-electron faradic reaction of oxidation of Pb(II) to Pb(IV) and vice versa

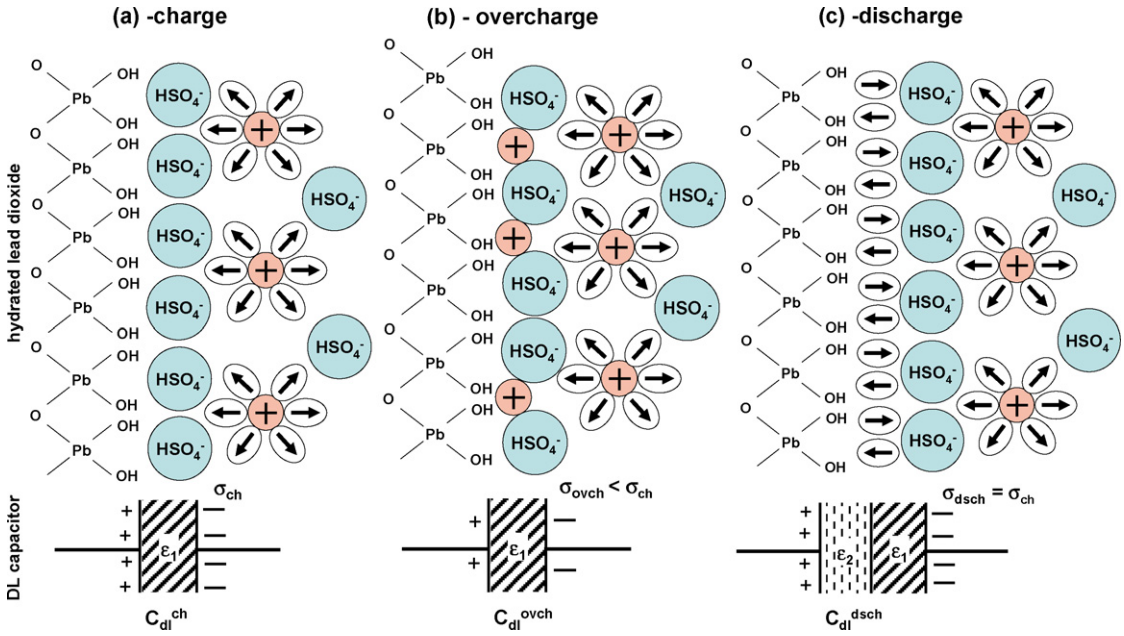

Fig. 11. Model of the EDL on the surface of the hydrated lead dioxide during the charge (a), the overcharge (b) and the discharge (c). The surface density of the charges (C m^{-2}) is denoted as σ_{ch}, σ_{ovch} and σ_{dsch} for the charge, the overcharge and the discharge. The water dipoles are denoted with arrows and the H^+ ions with "+".

(Eqs. (3b) and (4b)). The charge transfer resistance depends in a large extent on the properties of the active centres where the electrochemical reactions take place, i.e. on the properties of the gel part of the lead dioxide—its hydration, the content of ions of the positive grid alloying components like Sb, Sn, Bi, Ca, Ag etc. The dependence of the charge transfer resistance on SoC is shown in Fig. 12. This charge transfer resistance remains around 2 mΩ, but the deviation form this number can be substantial. In some cases, its measurement was impossible or the statistical error provided by *Z*-View2 software was between 50 and 100%. In these cases, in the DIA temporal plot the low-frequency, flat part of the R_{eff} was not available due to its location out of the studied frequency domain. These are the same cases where the C_{dl} featured a maximal values.

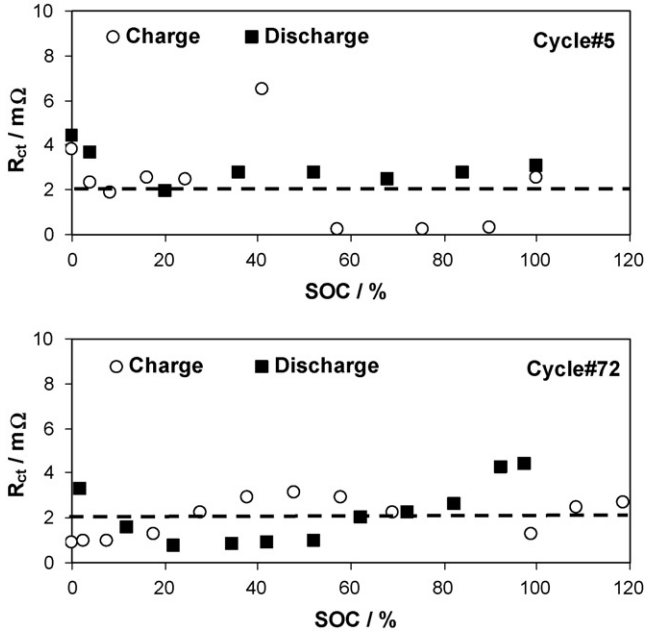

Fig. 12. Dependence of the charge transfer resistance R_{ct} on state of charge for a cell after 5 cycles and for a cell after 72 cycles with 100% DOD at 10 h rate of the charge and the discharge (0.8 A).

3.5.4. Evolution of the diffusion CPE

Typical data of the evolution of the parameters *T* and *P* (from Eq. (1)) of the diffusion constant phase element CPE_{diff} are presented in Fig. 13.

In general the parameter *T* accounts of how much the diffusion of the species included in the electrochemical process is facilitated. The values of *T* during the charge are markedly higher than in the case of the discharge, and qualitatively they follow the behaviour of the C_{dl} versus SoC. The explanation should be searched in the difference in the electrochemical reactions during of the charge and the discharge. The electrochemical reaction of the charge is given by Eq. (3b), where the diffusion process is associated with the transport of the Pb^{2+} ions from the surface of the $PbSO_4$ crystal to the closest active centre on the surface of the hydrated lead dioxide, i.e. the whole electrochemical process proceeds in the solution. The electrochemical reaction of the discharge is given by Eq. (4b). This reaction can proceed both on the surface and in the volume of the hydrated lead dioxide by solid-state diffusion of H^+ in the lead dioxide [61] especially when the surface is covered with $Pb(OH)_2$ or orthorhombic-PbO which is not electrochemically active [41].

The difference in the mechanisms of the diffusion processes is demonstrated even more clearly in the dependence of the *P*-coefficient—during the discharge the dependence of *P* on SoC is shifted towards lower values, closer to 0.5, which corresponds to semi-infinite diffusion of species described by the

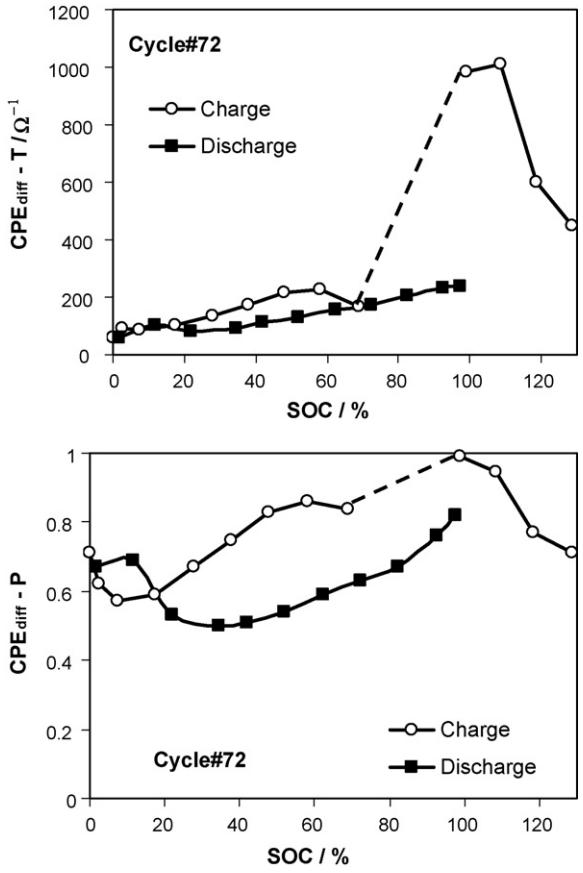

Fig. 13. Dependence of the diffusion-CPE parameters on state of charge for a cell subjected to 72 cycles.

Warburg element. The values of P are much closer to 1 during the charge, which puts the positive electrode quite closer to a supercapacitor type of electrode. This supports the hypothesis that the electrochemical reaction during the charge is rather surface (2D) than volume (3D) process. Similar type of spectra were measured three decades ago by Keddam et al. [62]. Separated EIS experiments of partially charged positive plates carried out down to 1 mHz confirmed that the values of P remain close to 1. The dependence of the CPE_{diff} parameters on SoC reflects the dynamics of the pore-distribution in the positive active material during the charge and the discharge, and the proposal of a more precise model requires EIS measurements to lower frequencies coupled with porometric data of PAM at different SoC during charge and during discharge.

3.5.5. Evolution of the parameters associated with the gel part of the lead dioxide

The dependence of the resistance, capacitance and time constant of the gel part (or hydrated part) of the lead dioxide on SoC is shown in (Fig. 14). The process corresponding to this circuit is the transfer of electrons through semiconductor type medium. The values of R_{gel} for the charge were estimated graphically from the Nyquist plots as the first semi-circle diameter, while the values of C_{gel} were estimated approximately from the DIA temporal plots in the same frequency range. The reason for this approach was due to fact that inductance error caused by the grids and the active materials shifted partially or completely the loop of the gel part of the lead dioxide in the inductive domain of the spectrum ($Z'' > 0$), and Z-View2 fitting was impossible.

During the whole charge, R_{gel} remains almost about 0.1 mΩ or less (the missing points correspond to zero values). The values of R_{gel} during the discharge are markedly higher and they increase, when increasing the depth of discharge. In the end of the discharge, the value of R_{gel} is more than one decade higher than in the beginning. It is obvious that this resistance corresponds to the partially discharged corrosion layer + AMCL instead of the gel part of the lead dioxide which is completely depleted in this moment.

A similar picture can be observed in C_{gel} versus SoC plot—during the discharge C_{gel} values (and hence the dielectric properties of the hydrated lead dioxide) are markedly higher.

Rate of the process of electronic transfer trough the gel can be represented also by its time constant T_{gel}. The best advantage of T_{gel} is that this parameter is independent of the electrode surface. The values of T_{gel} for the discharge are nearly two decades higher than for the charge, i.e. the process of the electron transfer through the hydrated lead dioxide during the discharge is quite slower. The dielectric properties of the hydrated lead dioxide are determined by its degree of hydration. Following the same logic used to explain the evolution of C_{dl} during the charge and the discharge we can assume that during the charge, the lead dioxide is subjected to dehydration, i.e. the dielectric properties of the gel part of the dioxide will be reduced and the electron transfer will be facilitated. During the discharge, the situation is opposite—H^+ ions and H_2O molecules penetrate

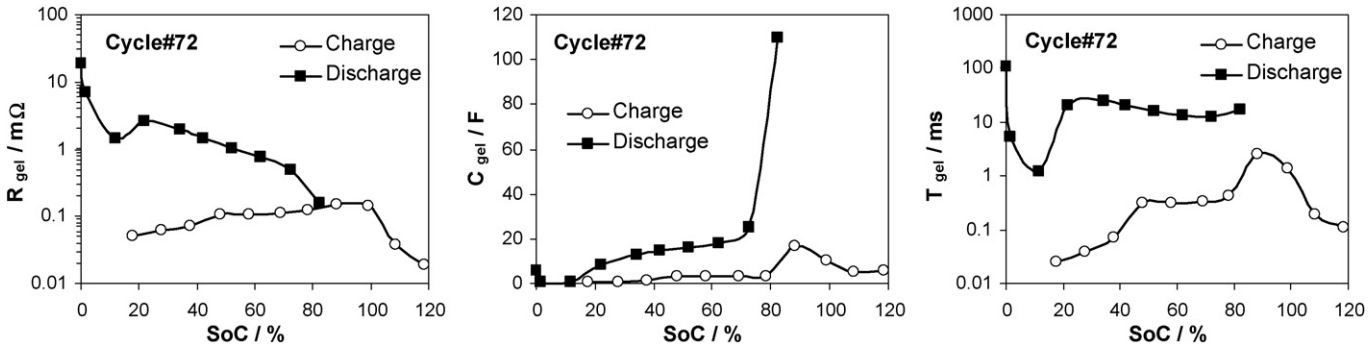

Fig. 14. Dependence of the elements of the circuit describing the impedance of the hydrated part of the lead dioxide for cell subjected to 72 cycles.

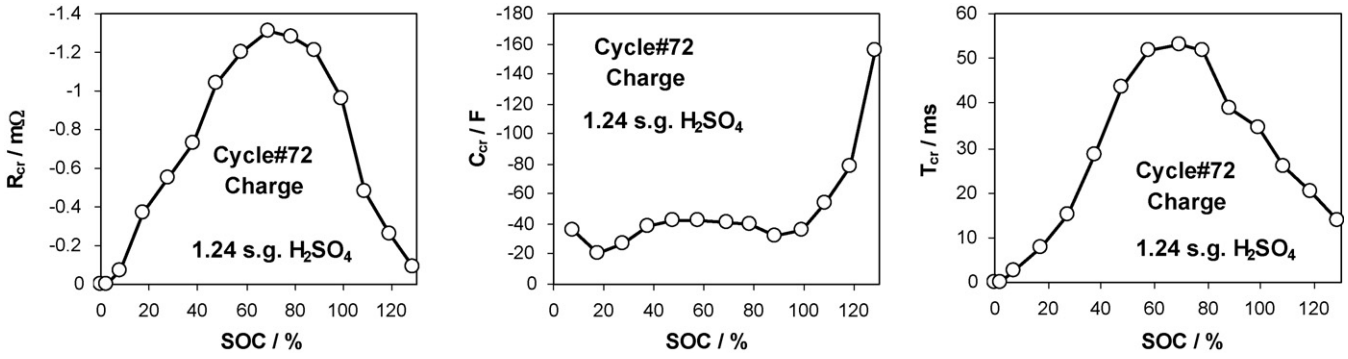

Fig. 15. Dependence of the elements of the circuit describing the impedance of the chemical reactions during the charge of the positive plate in a cell subjected to 72 cycles in 1.24 s.g. H_2SO_4.

in the PAM particles increasing their hydration. The result is an increase in the dielectric properties—higher resistance and higher electrostatic capacitance. The extremely high value of C_{gel} in the beginning of the discharge coincides with a result reported by Pavlov in [42]—he estimated by X-ray diffraction that the ratio crystal/gel shows a maximum in the beginning of the discharge, i.e. in the beginning of the discharge the thickness of the hydrated dioxide decreases while the quantity of the crystalline lead dioxide remains rather constant. The reduced thickness of the hydrated dioxide will increase substantially its electrostatic capacitance, considering the gel layer as a plain-parallel capacitor.

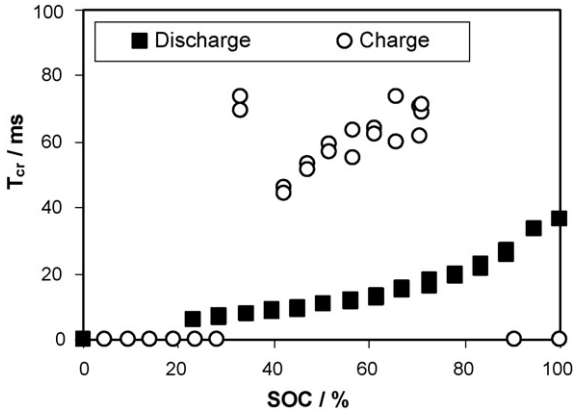

Fig. 16. Dependence of the pseudo-inductive time constant T_{cr} describing the impedance of the chemical reactions during the charge and the discharge of the positive plate in a cell subjected to 10 cycles in 1.28 s.g. H_2SO_4.

3.5.6. Evolution of the parameters associated with the chemical reactions during the charge of the positive plate in H_2SO_4 with s.g. 1.24 g ml^{-1}

The evolution with SoC of the negative resistance R_{cr}, negative capacitance C_{cr} and the corresponding time constant T_{cr}, which are result from the existence of chemical reactions during the conversion of the $PbSO_4$ to PbO_2, is shown in Fig. 15. The values of those time constants are reversely proportional to the rate of the chemical reactions and they do not depend on the electrode surface. In the beginning of the charge, T_{cr} increases, i.e. the chemical reactions rates decrease. This result can be associated with progression of the charge process from the surface of the plate and the biggest macropores towards the volume of the plate and the micropores, where the electrolyte transport can be slower. The maximum in T_{cr} versus SoC coincides approximately with the beginning of the oxygen evolution. A possible explanation for this acceleration of the chemical reactions is the formation of bubbles of oxygen in the pores of PAM, which

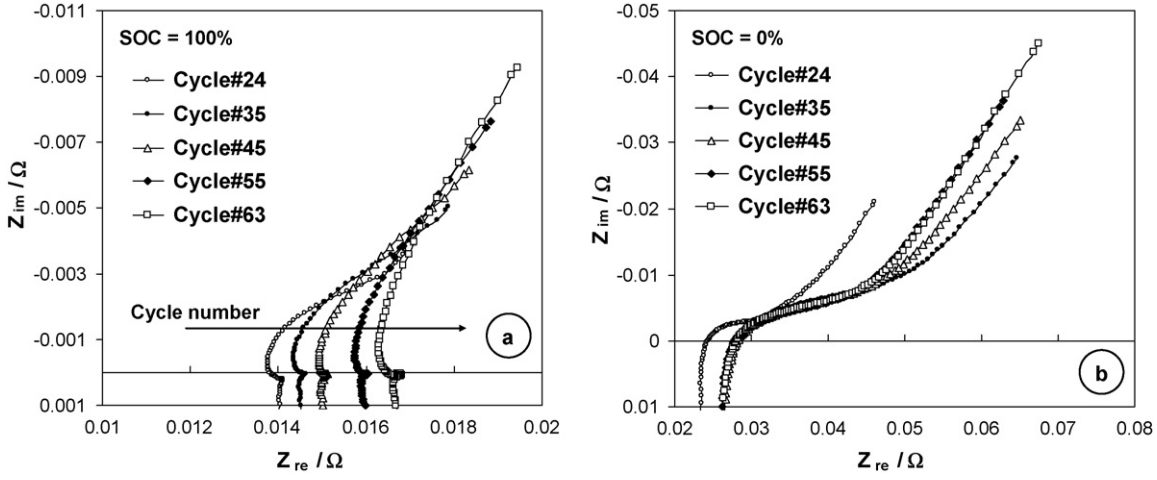

Fig. 17. Evolution of the impedance spectrum of the positive plate in charged (a) and in discharged (b) state. The data are not subjected to L-correction.

decrease the acid concentration gradients due to their movement in the plate and hence increase the rate of the $Pb(OH)_4$ dehydration.

3.5.7. Evolution of the parameters associated with the chemical reactions during the discharge of the positive plate in H_2SO_4 with s.g. 1.28 g ml^{-1}

A pseudo-inductive loop in the impedance spectra during the discharge and the charge was observed only in H_2SO_4 solutions with s.g. 1.28 g ml^{-1}. The dependence of T_{cr} on SoC for this case is shown in Fig. 16. The values of T_{cr} during the discharge are twice lower compared to those for the charge.

It was mentioned that the pseudo-inductive loop in the impedance spectra can be regarded also as a detection of passivation phenomenon. During the discharge, this can be formation of $Pb(OH)_2$ and orthorhombic-PbO, which cannot be converted to $PbSO_4$. Also recent studies showed that when the electrolyte density is higher than or equal to 1.28 s.g., the discharge capacity decreases compared to s.g. 1.24 g ml^{-1}, where the capacity is maximal [56]. The morphology of the lead dioxide and the α/β ratio also changes dramatically from electrolytes with s.g. 1.24–1.28 g ml^{-1}: the deposits, obtained in electrolyte with s.g. 1.28 g ml^{-1} by Planté cycling, present much less surface and much more α-PbO_2 and tetragonal-PbO, compared with deposits obtained in electrolytes with s.g. 1.24 g ml^{-1}: where the obtained anodic layers are thicker, with developed surface and built mainly by β-PbO_2 [53–55].

The appearance of the pseudo-inductive time constant during the cycling in the more concentrated electrolyte and its absence in more diluted electrolyte shows that loss of electrochemical activity is due to difficulties during the discharge, rather than during the charge. The similarities in the T_{cr} versus SoC dependence during the charge in both electrolytes show that the chemical processes during the charge cannot be considered as like passivation, regardless of the fact that they are slower compared with T_{cr} for the discharge.

3.6. Evolution of the equivalent circuit parameters during the cycling—influence of the state of health on the impedance data

In order to estimate the influence of the state of health on the equivalent circuit parameter values, a positive plate was subjected to cycling in electrolyte with s.g. 1.24 g ml^{-1} with increased charge factor (∼120%) and the impedance spectrum was measured after each charge and discharge. The capacity decay in this case was caused by softening and shedding of the active material due to the increased gassing. Fig. 17 presents the evolution of the impedance spectra for charged (a) and discharged (b) positive plate, the data is shown before the L-correction. Obviously, the completely charged state is a much better choice for a reference point in the state of health estimation, because the spectra show much more expectable differences. The presence of the time constants of the gel part of the lead dioxide and of the chemical reaction is also visible, but the semi-circuits are quite depressed. The results of the *Z*-View fitting with the corresponding equivalent circuits are listed in Tables 3a and 3b.

Table 3a
Charged positive plate

Cycle number	25	30	35	40	45	50	55	60	63
C_{dsch} (Ah)	7.08	6.76	6.1	5.49	4.54	3.84	3.14	2.78	2.15
R_Ω (mΩ)	7.61	7.97	7.93	8.30	8.59	8.80	9.41	9.62	10.13
R_{ct} (mΩ)	4.69	5.82	5.93	7.00	7.59	8.81	10.53	12.40	15.59
$CPE_{diff} - T$ (Ω^{-1})	384	307	271	242	193	156	123	101	91.5
$CPE_{diff} - P$	0.89	0.83	0.82	0.83	0.80	0.78	0.75	0.73	0.76
C_{dl} (F)	103.6	105.4	328.0	263.1	260.8	223.3	315.7	250.0	211.4
$CPE_{gel} - T$ (Ω^{-1})	n.a.	n.a.	1.79	3.44	4.72	4.13	2.91	2.19	2.64
$CPE_{gel} - P$	n.a.	n.a.	1	1	1	1	1	1	1
R_{gel} (mΩ)	n.a.	n.a.	0.408	0.331	0.316	0.337	0.387	0.453	0.429
$CPE_{cr} - T$ (Ω^{-1})	n.a.	n.a.	−206	−138	−134	−94.8	−183	−119	−88.7
$CPE_{cr} - P$	n.a.	n.a.	1	1	1	1	1	1	1
R_{cr} (μΩ)	n.a.	n.a.	−42	−65	−69	−119	−62	−135	−203

Table 3b
Discharged positive plate

Cycle number	25	30	35	40	45	50	55	60	63
C_{dsch} (Ah)	7.08	6.76	6.1	5.49	4.54	3.84	3.14	2.78	2.15
R_Ω (mΩ)	14.35	14.46	15.95	16.36	13.87	15.18	14.50	14.33	14.93
R_{ct} (mΩ)	48.89	2.34	2.45	2.84	3.02	67.2	63.7	82.36	62.34
$CPE_{diff} - T$ (Ω^{-1})	33.53	53.47	52.32	45.82	39.06	28.85	23.5	23.41	19.35
$CPE_{diff} - P$	0.93	0.73	0.75	0.73	0.71	0.75	0.75	0.84	0.80
C_{dl} (F)	55.74	5.00	6.90	6.25	5.05	43.99	40.29	34.73	30.71
$CPE_{ic} - T$ (Ω^{-1})	21.42	12.92	11.38	10.62	11.95	14.03	14.48	14.05	12.06
$CPE_{ic} - P$	0.24	0.27	0.30	0.30	0.25	0.26	0.25	0.26	0.27
R_{ic} (mΩ)	99.71	41.08	45.09	41.58	41.84	62.0	59.4	56.7	55.2

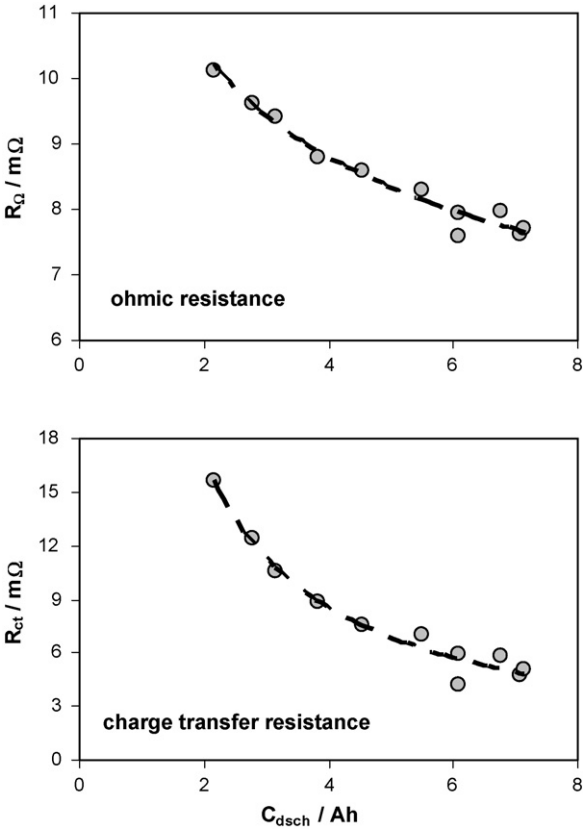

Fig. 18. Dependence of the ohmic resistance and the charge transfer resistance on the discharge capacity at SOC = 100%.

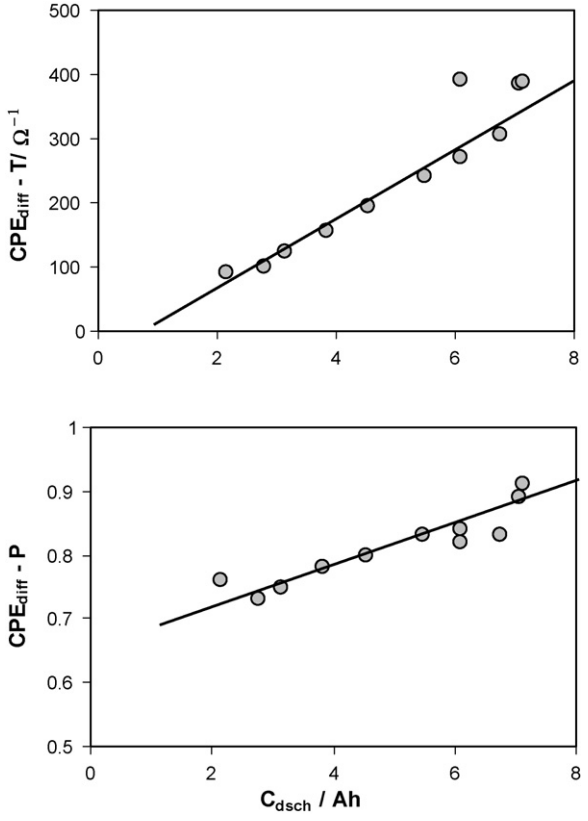

Fig. 19. Dependence of the diffusion CPE parameters on the discharge capacity at SOC = 100%.

According to the obtained data there are two suitable parameters which are sensitive to the SoH of the positive plate. These are the ohmic resistance R_Ω and the charge transfer resistance R_{ct}. The plots of R_Ω and R_{ct} versus the discharge capacity are shown in Fig. 18. Similar are the plots of R_Ω and R_{ct} versus the cycle number. The obtained results show that the charge transfer resistance is the more sensitive parameter when the failure mode is degradation of the active material by softening and shedding.

Another parameter which "drags attention" is CPE_{diff}. The dependence of its two parameters on the discharge capacity is shown in Fig. 19. Both T and P decrease with the capacity decay of the plate. Here the interpretation of the obtained plots is even harder, because CPE is an empiric parameter. One is sure—the softening of the PAM alters markedly its pore-distribution and hence the mechanism of the electrolyte diffusion inside the positive plate.

4. Conclusions

The EIS results obtained for partially charged and partially discharged lead-acid battery positive plates and their interpretation by differential impedance analysis and equivalent circuit modelling support well the gel-crystal model of the lead dioxide. The existing equivalent circuit models describing the impedance of the positive plate in 0 and in 100% SoC were extended with parameters accounting the influence of the gel part of the lead dioxide and the presence of chemical reactions included in the charge and discharge process. The evolution of the element values of the equivalent circuits during the charge and the discharge in two different electrolytes show clearly the differences in the mechanisms of the charge and the discharge process, i.e. they are not just same process taking place in opposite direction. Using the reaction mechanism developed in the frames of the gel-crystal model, the observed huge hysteresis of the EDL capacitance during the charge/discharge cycle was explained. Three types of structure of EDL were proposed—for the charge, for the overcharge when the oxygen evolution takes place and for the discharge. It was found that the increase of the electrolyte concentration could decrease the rate of the chemical processes during the discharge, which explains, in terms of passivation, why the capacity of the positive plate decreases in more concentrated electrolytes. The results obtained from the study of the relation between EIS and state of health showed that the better mode for SoH estimation by EIS is when the positive plate is well charged. In this case the parameters, which are sensitive to SoH are the ohmic resistance, the charge transfer resistance and both parameters of the diffusion CPE.

We can conclude that in a short time scale (one charge–discharge cycle) the behaviour of the impedance of the positive plate is determined by the double layer effects and the diffusion effects caused by the changes in the porosity. In long time scale (cycling and ageing) the EDL effects are supplanted by changes in the charge transfer resistance and the ohmic resistance. The evolution of the values of CPE_{diff} during the cycling and ageing reflects the changes in the skeleton structure of PAM, which is also connected to the diffusion effects.

References

[1] A. Kirchev, M. Perrin, E. Lemaire, F. Karoui, F. Mattera, J. Power Sources, in press.
[2] M. Keddam, C. Rakotomavo, H. Takenouti, Proc. Electrochem. Soc. 84 (14) (1984) 277–287.
[3] M. Hughes, R.T. Barton, S.A.G.R. Karunathilaka, N.A. Hampson, J. Power Sources 17 (1986) 305–329.
[4] M. Hughes, R.T. Barton, S.A.G.R. Karunathilaka, N.A. Hampson, J. Appl. Electrochem. 16 (1986) 555–564.
[5] F. Boettcher, H.S. Panesar, J. Power Sources 36 (1991) 439–450.
[6] V.V. Viswanathan, A.J. Salkind, J.J. Kelley, J.B. Ockerman, J. Appl. Electrochem. 25 (1995) 729–739.
[7] F. Huet, J. Power Sources 70 (1998) 59–69.
[8] E. Karden, S. Buller, R.W. De Doncker, J. Power Sources 85 (2000) 72–78.
[9] E. Karden, R.W. De Doncker, Proceedings of the Conference INTELEC 2001, Edinburgh, UK, October 14–18, 2001, pp. 65–72.
[10] E. Karden, Using low-frequency impedance spectroscopy for characterization, monitoring, and modeling of industrial batteries, Ph.D. Thesis, Aachen, Germany, 2001.
[11] B.N. Kabanov, I.G. Kiseleva, D.I. Leykis, Dokl. Acad. Nauk SSSR (Rus.) 99 (1954) 805.
[12] I.G. Kiseleva, B.N. Kabanov, Dokl. Acad. Nauk SSSR 108 (1956) 864.
[13] J.P. Carr, N.A. Hampson, R. Taylor, J. Electroanal. Chem. 27 (1970) 201–206.
[14] N. Munichandraiah, J. Electroanal. Chem. 266 (1989) 179–184.
[15] N. Munichandraiah, J. Appl. Electrochem. 22 (1992) 825–829.
[16] P. Ruetschi, J. Power Sources 116 (2002) 53.
[17] P. Ruetschi, J. Power Sources 113 (2002) 363.
[18] D. Benchetrite, M. Le Gall, O. Bach, M. Perrin, F. Mattera, J. Power Sources 144 (2005) 346–351.
[19] D. Vladikova, Z. Stoynov, G. Raikova, in: D. Vladikova, Z. Stoynov (Eds.), Portable and Emergency Energy Sources, Prof. Marin Drinov Academic Publishing House, Sofia, 2006.
[20] G. Raikova, D. Vladikova, Z. Stoynov, Impedance Contributions Online 3 (2005) P7 (e-journal, http://accessimpedance.iusi.bas.bg).
[21] Z. Stoynov, D. Vladikova, Differential Impedance Analysis, Prof. Marin Drinov Academic Publishing House, Sofia, 2005.
[22] Z. Stoynov, Electrochim. Acta 34 (1989) 1187–1192.
[23] Z. Stoynov, Polish J. Chem. 71 (1997) 1204–1210.
[24] D. Vladikova, P. Zoltowski, E. Makowska, Z. Stoynov, Electrochim. Acta 47 (2002) 2943–2951.
[25] D. Vladikova, Z. Stoynov, J. Electroanal. Chem. 572 (2004) 377–387.
[26] D. Vladikova, Z. Stoynov, L. Ilkov, Polish J. Chem. 71 (1997) 1196–1203.
[27] D. Vladikova, Z. Stoynov, M. Viviani, J. Eur. Ceram. Soc. 24 (2004) 1121–1127.
[28] D. Vladikova, G. Raikova, Z. Stoynov, H. Takenouti, J. Kilner, St. Skinner, Solid State Ionics 176 (2005) 2005–2009.
[29] A. Barbucci, P. Carpanese, M. Viviani, P. Piccardo, D. Vladikova, Z. Stoynov, Proceedings of the First European Fuel Cell Technology and Applications Conference, 2005, p. 109.
[30] D. Vladikova, J.A. Kilner, S.J. Skinner, G. Raikova, Z. Stoynov, Electrochim. Acta 51 (2006) 1611–1621.
[31] A. Barbucci, M. Viviani, P. Carpanese, D. Vladikova, Z. Stoynov, Electrochim. Acta 51 (2006) 1641–1650.
[32] M. Cabeza, P. Merino, A. Miranda, X.R. Nóvoa, I. Sanchez, Cement Concrete Res. 32 (2002) 881–891.
[33] P. Zoltowski, J. Electroanal. Chem. 443 (1998) 149–154.
[34] C.H. Hsu, F. Mansfeld, Corrosion 57 (2001) 747–748.
[35] V.D. Jovic, Published on-line at http://www.gamry.com, November 2003.
[36] D. Pavlov, G. Petkova, J. Electrochem. Soc. 149 (2002) A654–A661.
[37] R. De Marco, A. Lowe, M. Sercombe, P. Singh, Electrochim. Acta 51 (2006) 2088–2095.
[38] B.E. Conway, J. Electrochem. Soc. 138 (1991) 1539–1548.
[39] J. Niu, B.E. Conway, W.G. Pell, J. Power Sources 135 (2004) 332–343.
[40] D. Pavlov, E. Bashtavelova, V. Manev, A. Nasalevska, J. Power Sources 19 (1987) 15–25.
[41] D. Pavlov, I. Balkanov, P. Rachev, J. Electrochem. Soc. 134 (1987) 2390–2398.
[42] D. Pavlov, I. Balkanov, T. Halachev, P. Rachev, J. Electrochem. Soc. 136 (1989) 3189–3197.
[43] D. Pavlov, I. Balkanov, J. Electrochem. Soc. 139 (1992) 1830–1835.
[44] D. Pavlov, J. Electrochem. Soc. 139 (1992) 3075–3085.
[45] D. Pavlov, J. Power Sources 42 (1993) 345–363.
[46] D. Pavlov, J. Power Sources 46 (1993) 171–190.
[47] B. Monahov, D. Pavlov, J. Appl. Electrochem. 23 (1993) 1244–1250.
[48] B. Monahov, D. Pavlov, J. Electrochem. Soc. 141 (1994) 2316–2326.
[49] D. Pavlov, J. Power Sources 53 (1995) 9–21.
[50] D. Pavlov, Electrochim. Acta 13 (1968) 2051–2061.
[51] D. Pavlov, in: L.J. Pearce (Ed.), Power Sources-11, 15th International Symposium, Brighton, 1986, Pergamon Press, London, 1987, p. 165.
[52] D. Pavlov, I. Pashmakova, J. Appl. Electrochem. 17 (1987) 1075–1082.
[53] B. Monahov, A. Kirchev, S. Vasilev, D. Pavlov, Proceedings of the International Conference LABAT-02, Sofia, June, 2002, pp. 51–56.
[54] B. Monahov, D. Pavlov, A. Kirchev, S. Vasilev, J. Power Sources 113 (2003) 281–292.
[55] D. Pavlov, A. Kirchev, M. Stoycheva, B. Monahov, J. Power Sources 137 (2004) 288–308.
[56] D. Pavlov, V. Naidenov, S. Ruevski, J. Power Sources 161 (2006) 658–665.
[57] P. Ruetschi, International Patent WO2004019022 (March 4, 2004).
[58] F. Huet, R.P. Nogueira, P. Lailler, L. Torcheux, J. Power Sources 158 (2006) 1012–1018.
[59] T. Hiemstra, W.H. Van Riemsdijk, J. Colloid Interf. Sci. 297 (2006) 379–388.
[60] M.A. Henderson, Surf. Sci. Rep. 46 (2002) 1–308.
[61] L. Zerroual, R. Fitas, B. Djellouli, N. Chelali, J. Power Sources 158 (2006) 837–840.
[62] M. Keddam, Z. Stoynov, H. Takenouti, J. Appl. Electrochem. 7 (1977) 539–544.